iScience

CellPress
OPEN ACCESS

Article

Immunomodulatory potential of *in vivo* natural killer T (NKT) activation by NKTT320 in Mauritian-origin cynomolgus macaques

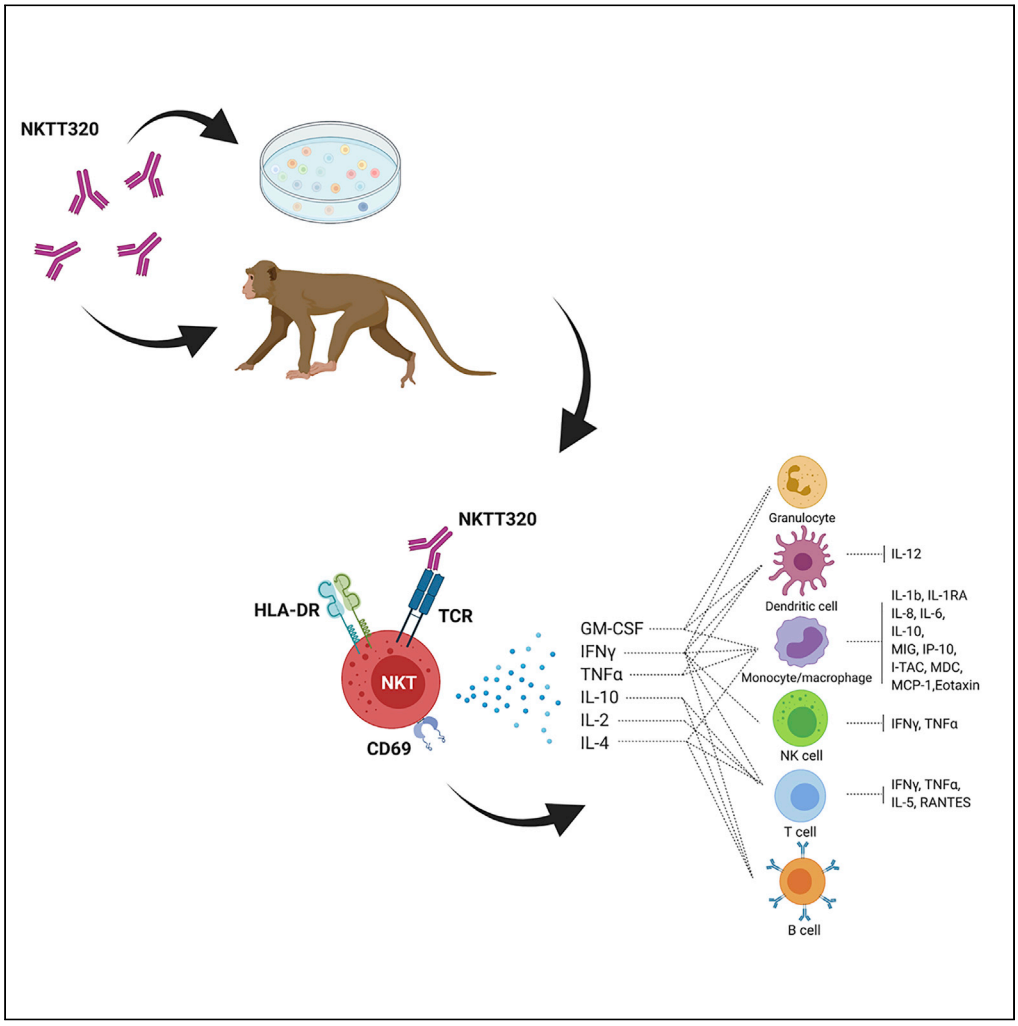

Nell G. Bond, Marissa D. Fahlberg, Shan Yu, ..., Joseph C. Mudd, Robert Schaub, Amitinder Kaur

akaur@tulane.edu

Highlights

NKTT320 rapidly activates iNKT *in vivo*, modulating downstream immune function

In vivo NKTT320 treatment modulates pro- and anti-inflammatory genes

NKTT320 treatment results in activation of innate and adaptive immune subsets

NKTT320 has promise as an immunotherapeutic with translational potential

Bond et al., iScience *25*, 103889
March 18, 2022
https://doi.org/10.1016/j.isci.2022.103889

iScience

CellPress
OPEN ACCESS

Article

Immunomodulatory potential of *in vivo* natural killer T (NKT) activation by NKTT320 in Mauritian-origin cynomolgus macaques

Nell G. Bond,[1] Marissa D. Fahlberg,[1] Shan Yu,[1] Namita Rout,[1] Dollnovan Tran,[1] Taylor Fitzpatrick-Schmidt,[1] Lesli M. Sprehe,[1] Elizabeth A. Scheef,[1] Joseph C. Mudd,[1] Robert Schaub,[2] and Amitinder Kaur[1,3,*]

SUMMARY

Invariant natural killer T-lymphocytes (iNKT) are unique immunomodulatory innate T cells with an invariant TCRα recognizing glycolipids presented on MHC class-I-like CD1d molecules. Activated iNKT rapidly secrete pro-and anti-inflammatory cytokines, potentiate immunity, and modulate inflammation. Here, we report the effects of *in vivo* iNKT activation in Mauritian-origin cynomolgus macaques by a humanized monoclonal antibody, NKTT320, that binds to the invariant region of the iNKT TCR. NKTT320 led to rapid iNKT activation, increased polyfunctionality, and elevation of multiple plasma analytes within 24 hours. Flow cytometry and RNA-Seq confirmed downstream activation of multiple immune subsets, enrichment of JAK/STAT and PI3K/AKT pathway genes, and upregulation of inflammation-modulating genes. NKTT320 also increased iNKT frequency in adipose tissue and did not cause iNKT anergy. Our data indicate that NKTT320 has a sustained effect on *in vivo* iNKT activation, potentiation of innate and adaptive immunity, and resolution of inflammation, which supports its future use as an immunotherapeutic.

INTRODUCTION

Invariant Natural Killer T (iNKT) lymphocytes are rare, innate T-lymphocytes with unique antigen recognition and immunomodulatory properties that make up approximately 0.01–0.1% of circulating T-lymphocytes in humans (Berzins et al., 2011). iNKT were first discovered in mice during anti-tumor studies and named for the expression of the natural killer (NK) marker NK1.1 on T-lymphocytes. iNKT differ from classical T lymphocytes in multiple distinct, important ways. iNKT express a conserved T-cell receptor (TCR) Vα chain with an invariant complementary determining region 3 (CDR3α) as opposed to the polymorphic TCR on classical T-lymphocytes. Primate iNKT express Vα24-Jα18 which preferentially pairs with a restricted repertoire of Vβ subunits, generally Vβ11 (Bendelac et al., 2007). In contrast with classical T lymphocytes, iNKT recognize and are rapidly activated by both endogenous and exogenous glycolipid antigens presented by antigen presenting cells (APCs) on nonpolymorphic MHC-class-I-like CD1d molecules. The classical, most widely studied iNKT activating lipid antigen is alpha-galactosylceramide (αGC), derived from the marine sponge *Agelas mauritianus* and first identified in murine cancer studies (Berzins et al., 2011). Upon activation, iNKT rapidly produce a wide range of cytokines covering T helper (Th) 1, Th2 and Th17 functionality, often from the same cell (Van Kaer et al., 2015). iNKT in primates are more strictly defined by co-staining of the αGC-loaded CD1d tetramer (CD1dTM) and Vα24 on $CD3^+$ T-lymphocytes (Watarai et al., 2008; Rout et al., 2010).

Because of their rapid response and broad functional potential, iNKT bridge the gap between innate and adaptive immunity (Brennan et al., 2013). Once activated, iNKT can be directly cytolytic (through perforin and granzyme B) and display Th1, Th2 and Th17 effector functions. Additionally, iNKT rapidly influence the function of multiple immune subsets (Brennan et al., 2013). Bidirectional interactions between iNKT and dendritic cells (DC) enhances DC maturation and facilitates antigen cross-presentation and priming of antigen-specific T-lymphocyte responses (Fujii et al., 2004; Stober et al., 2003). Activated iNKT can potentiate macrophage phagocytic function and affect polarization (Brennan et al., 2013). IFNγ production by iNKT rapidly activates natural killer (NK) cells improving cytolysis (Carnaud et al., 1999). Finally, iNKT are known to recruit and provide help to B cells, improving B cell maturation, antibody class switching, and overall

[1]Tulane National Primate Research Center, Division of Immunology, Covington, LA 70433, USA

[2]RGS Consulting, Pelham, NH 03076, USA

[3]Lead contact

*Correspondence: akaur@tulane.edu

https://doi.org/10.1016/j.isci.2022.103889

humoral immunity (Chang et al., 2011; King et al., 2011). Because of their diverse immunomodulatory properties, there is great interest in harnessing iNKT activation as an immunotherapeutic tool and a vaccine adjuvant.

Studies exploring αGC-mediated iNKT activation as an immunomodulatory tool and vaccine adjuvant have largely been conducted in mice with varying degrees of success (Kopecky-Bromberg et al., 2009; Gonzalez-Aseguinolaza et al., 2002; Fujii et al., 2003; Silk et al., 2004; Venkataswamy et al., 2009). One barrier to the use of iNKT activating agents such as soluble αGC *in vivo* in murine cells is subsequent iNKT anergy in which iNKT are rendered unable to respond to further stimuli (Fujii et al., 2002; Parekh et al., 2005). Reports on the efficacy of repeated *in vivo* administration of soluble αGC on potentiating iNKT function in humans are limited (Giaccone et al., 2002). Administration of αGC loaded on autologous DCs has shown great promise for cancer immunotherapy in human studies without inducing anergy (Kunii et al., 2009; Motohashi et al., 2011; Chang et al., 2005). Because of the limitations in use of soluble αGC, alternate strategies of *in vivo* iNKT activation that can effectively harness the immunomodulatory properties of iNKT for widespread therapeutic use are warranted.

Antibodies directed against the iNKT cell receptor are one such class of potential iNKT modulating agents. NKTT120 is a humanized monoclonal iNKT depleting antibody developed by NKT Therapeutics (Sharon, MA) that directly binds to the CDR3 region of the Vα−subunit of the semi-invariant iNKT TCR with high affinity (Scheuplein et al., 2013). NKTT120 was engineered with an IgG1 Fc, thus supporting Fc-receptor binding and iNKT depletion by antibody dependent cellular cytotoxicity (ADCC) (Scheuplein et al., 2013). NKTT120 successfully depleted iNKT without any adverse effects in healthy humans and macaques (Scheuplein et al., 2013; Field et al., 2017). The humanized monoclonal antibody NKTT320 developed by NKT Therapeutics shares the variable region and iNKT binding specificity with NKTT120 but was engineered with an IgG4 Fc (Scheuplein et al., 2013) allowing it to successfully bind and activate iNKT without ADCC-mediated depletion (Reddy et al., 2000; Patel et al., 2020). *In vitro* iNKT activation in response to NKTT320 has been characterized previously (Patel et al., 2020), however, the *in vivo* translational potential has yet to be described.

In this study, we characterized the *in vivo* effects of NKTT320 administration on iNKT function and bystander lymphocyte subsets in Mauritian-origin cynomolgus macaques (MCM). We show rapid induction of iNKT activation and polyfunctionality without anergy, downstream effects on monocytes, T- and B-lymphocytes, and gene enrichment in the inflammatory response, heme metabolism, JAK/STAT signaling and PI3K/AKT pathways. Our results demonstrate the utility of NKTT320 as an *in vivo* immunomodulatory tool with high translational promise.

RESULTS

NKTT320 specifically activates iNKT

To characterize the potential of NKTT320 as an immunomodulatory tool, we first conducted *in vitro* studies in unfractionated peripheral blood mononuclear cells (PBMCs) of MCM. MCM were chosen because their circulating iNKT frequencies and phenotype are more similar to humans than other NHP models (Rout et al., 2012). As previously reported, iNKT were identified by flow cytometry as T-lymphocytes binding to αGC-loaded CD1d-tetramers (CD1dTM) and co-expressing the Vα24 TCR (Rout et al., 2010, 2012) (Figures 1A and S1A). PBMCs stimulated *in vitro* with goat-*anti*-mouse-IgG (GAM-IgG) cross-linked NKTT320 at 200ng/mL showed specific iNKT activation as evidenced by CD3 downregulation, CD69 upregulation, and secretion of IFNγ and TNFα compared to media alone (Figures 1B and S1B). Escalating concentrations of NKTT320 showed a dose-dependent effect on iNKT activation as indicated by downregulation of Vα24, CD1dTM, and CD3; and upregulation of CD69 (Figures 1C, 1D, S1C, and S1D). At higher doses, a combination of TCR downregulation and competition for the same invariant TCR binding site resulted in loss of sensitivity to detect CD1dTM-positive iNKT (Figure 1C). iNKT activation was not associated with non-NKT T-lymphocyte activation during a 24-h stimulation period demonstrating the iNKT specificity of NKTT320 (Figures 1B, 1D, S1C, and S1D).

We then evaluated *in vitro* NKTT320 treatment for differences in activation of single positive CD4 or CD8 iNKT. Unlike in humans, MCM iNKTs do not have a substantial CD4/CD8 double-negative population, so this population was not investigated (Rout et al., 2010). Unstimulated cultured $CD4^+$ and $CD8^+$ iNKT did not differ in baseline activation levels measured by surface CD69 and HLA-DR expression (Figure 1E and data not shown). NKTT320 treatment led to significant activation of both $CD4^+$ ($p = 0.0312$) and $CD8^+$ iNKT ($p =$

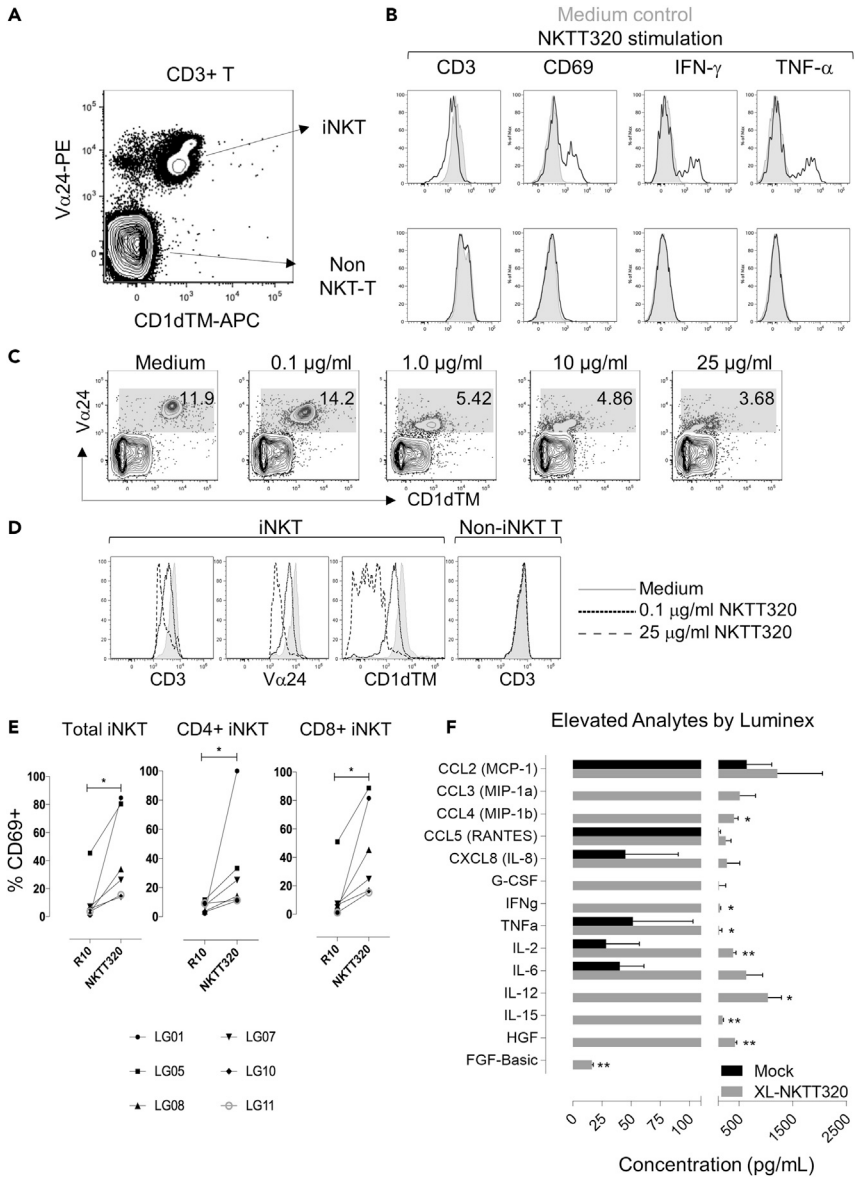

Figure 1. iNKTs are specifically activated by NKTT320

(A) Representative plot showing iNKT and non-NKT T cell gating strategy gated on $CD3^+$T-cells.

(B) Overlay histograms (unstimulated = shaded, NKTT320 = open histogram) comparing CD3, CD69 and cytokine expression on R10 and NKTT320 (200 ng/mL) treated PBMCs stimulated for 4hrs*in vitro*, iNKTs (top) and non-NKT T–cells (bottom).

(C and D) *In vitro* data showing iNKT frequency and TCR downregulation after overnight incubation with escalating concentrations of NKTT320. TCR downregulation is measured by Vα24, CD1d and CD3.

(E) $CD4^+$ and $CD8^+$ iNKT activation *in vitro* measured by CD69 in six animals stimulated with 200 ng/mL NKTT320 for 4 h.

(F) Luminex data showing analytes which were elevated in cells stimulated with 200 ng/mL NKTT320 compared with medium. Supernatants were collected after 48 h. Statistics were done by non-parametric Wilcoxon signed-rank test (n = 3). *<0.05, **<0.01. Mean and standard error of the mean (SEM) are shown. See also Figure S1

0.0312) as measured by CD69 upregulation (Figure 1E). There was no significant difference in activation of $CD4^+$ compared to $CD8^+$ iNKT (data not shown).

To examine broader functional changes resulting from NKTT320 treatment we cultured PBMC *in vitro* for 48 h with either media alone (mock stimulation) or with cross-linked NKTT320 and measured secreted

analytes using a non-human primate (NHP) 29-plex Luminex (Figures 1F and S1E). Analytes significantly elevated in the NKTT320-treated supernatants included proinflammatory and Th1 cytokines (IFNγ, TNFα, IL-12, IL-2, IL-15), chemokines (CCL4), and growth factors (FGF-basic, HGF). IL-6, CXCL8 (IL-8), CCL2, CCL3, and CCL5 (RANTES) trended higher but the increase did not reach statistical significance.

Differential effects of *in vitro* NKTT320 and aGC stimulation on iNKT function

Because glycolipid agonists are being used for iNKT activation, we compared NKTT320 to the classic iNKT agonist, αGC. In a series of time course *in vitro* stimulation experiments, all parameters of iNKT activation (CD69, IFNγ, TNFα, IL-2 and IL-4) appeared more rapidly and were of greater magnitude after NKTT320 as compared to αGC stimulation (Figures 2A, S2A, and S2B). Increased IFNγ and TNFα secretion, and increased iNKT polyfunctionality were apparent within 4 h of NKTT320 stimulation (Figures 2A and 2B). With the exception of IL-4, αGC-stimulated iNKT were able to match responses from NKTT320-stimulated cells by 48 h (Figure 2A). To determine effects on cytolytic function, we measured surface expression of CD107a and CD107b on iNKT and NK cells as a marker of degranulation. Following a six- and 13-h stimulation of PBMC from three macaques with NKTT320 or αGC, low frequencies of CD107a/b-positive degranulating iNKT were observed at 6-h after NKTT320 stimulation with a further increase at 13 h (Figure 2C). In contrast, αGC stimulation led to higher frequencies of CD107a/b-positive degranulating iNKT that were most evident by 13 h after stimulation (Figures 2C and S2C).

In the PBMC stimulation experiments we also looked at the effects of iNKT activation on NK function. NKTT320 stimulation resulted in an increase in NK activation but not cytolytic function as evidenced by increased frequencies of CD69-positive and IFNγ-secreting NK cells in the absence of NK degranulation (Figure S2D). The effect of C1Rd/αGC iNKT activation on NK function could not be assessed because C1R mock cell lines induced robust NK degranulation at levels similar to αGC-pulsed C1Rd cell lines likely because of recognition of non-self antigen (data not shown).

The differential effects of NKTT320 and αGC may have implications for choice of therapeutic use of NKT agonists based on purpose. A rapid, polyfunctional immune response such as that induced by NKTT320 might be preferred in situations where the induction of strong humoral and cellular responses is desired, such as a vaccine adjuvant. On the other hand, NKT agonists like αGC may be a better choice for immunotherapy of tumors where cytolytic function is needed.

NKTT320 effect on iNKT killing of CD1d-expressing target cells

Because NKTT320 action relies on antibody binding to the invariant region of the iNKT TCR, it is conceivable that its administration could result in iNKT no longer being able to bind or recognize glycolipid loaded CD1d-expressing cells, an effect that could abrogate iNKT killing of CD1d-expressing tumor cells or iNKT engagement with CD1d-expressing antigen-presenting cells. To assess the consequences of NKTT320 binding on the ability of iNKT to kill CD1d-expressing target cells, we performed two additional *in vitro* experiments; a calcein release kill assay of CD1d-expressing K562 target cell lines by *in vitro* expanded NKT cell effectors in the absence or presence of NKTT320; and an *ex vivo* degranulation assay of PBMC stimulated with αGC-pulsed C1Rd cells to measure apoptosis of C1Rd cells in the absence or presence of NKTT320.

First, we assessed direct killing by iNKT using a calcein release assay. iNKT of four MCMs were expanded *in vitro* by stimulation of PBMC with αGC-pulsed autologous irradiated PBMC at a 1:1 ratio for 10 days in the presence of IL-2. Stimulated cultures containing >95% T lymphocytes with 33–65% iNKT (Figure S3A and data not shown) were rested for 2–3 days with gradual reduction of IL-2 and then co-cultured for 6 h in the absence or presence of NKTT320 with Calcein AM labeled target cells consisting of αGC-pulsed A4.4 cells or control CD1d-null K562 cells. A4.4 cells (obtained from Dr Leonid Metelitsa, Baylor College of Medicine) are K562 cells stably transfected to express CD1d and costimulatory ligands CD86, 4-1BBL and OX40L and are similar to B-8-2 cells described by Tian et al. (2016). NKT cultures from all four animals lysed αGC-pulsed A4.4 cells at levels above K562 cells (Figure 3A). NKTT320 pre-incubation resulted in a 20- to 60% inhibition of lysis of αGC-pulsed A4.4 cells by NKT cultures from two animals (NK16 and NK17) with no inhibition observed in the other two animals (LG06 and NK19) (Figure 3A). The presence or absence of inhibition did not appear to be dependent on the frequency of iNKT in cultures, nor on the effector: target (E:T) ratio. Instead, we observed a direct relationship between % inhibition and % $CD8^+$ iNKT in culture (Figure S3B). iNKT cultures with killing activity unaffected by pre-incubation with

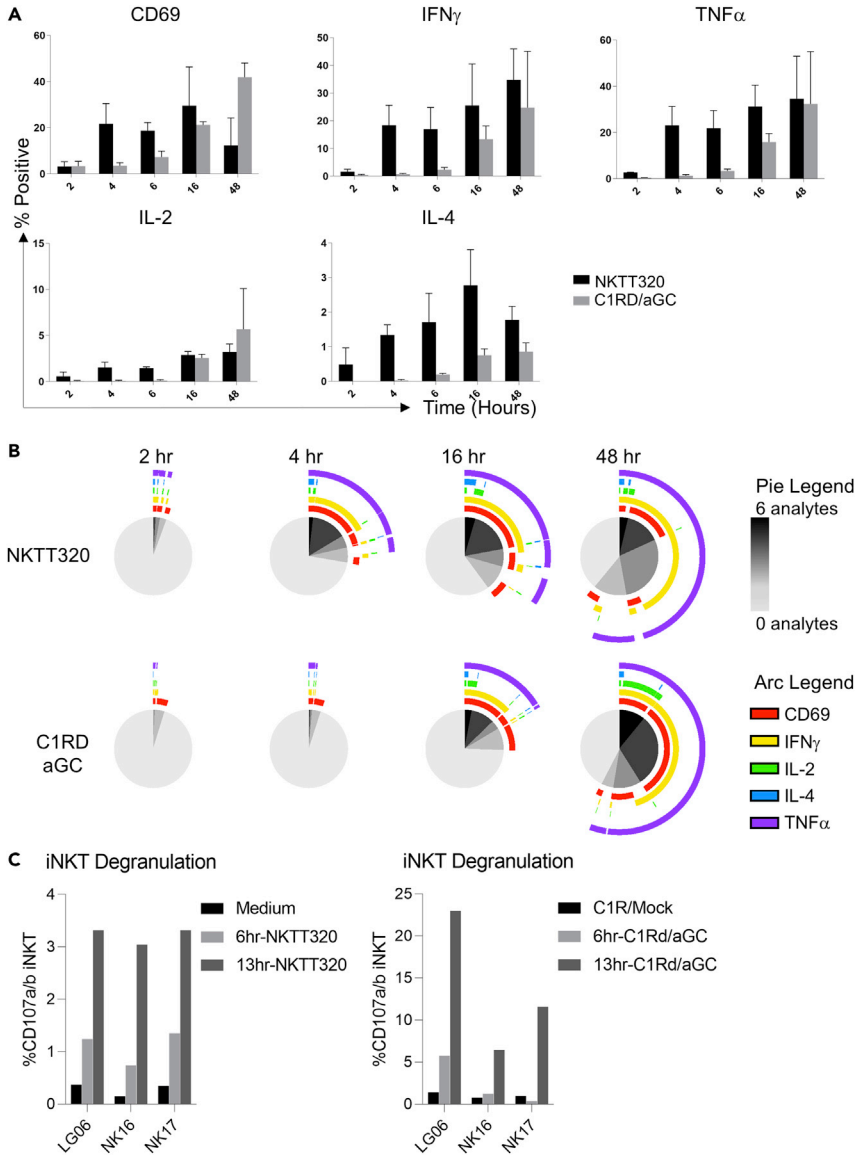

Figure 2. Comparison of iNKT activation by NKTT320 and αGC

(A) Intracellular cytokine staining of PBMCs stimulated with goat-*anti*-mouse-IgG cross-linked NKTT320 or αGC loaded on C1Rd cells, harvested and stained at 2, 4, 6, 16, and 48 h. Data on cytokine secretion gated on Vα24+ cells. Mean and SEM shown (n = 2).

(B) SPICE analysis of experiment described in (A) showing kinetic differences in speed, magnitude and co-expression of cytokines in NKTT320 and αGC stimulated iNKT cells (n = 2).

(C) Flow cytometry data depicting showing frequency of CD107a/b-positive degranulating iNKT in response to medium or 200 ng/mL NKTT320 (left panel), and C1R/Mock or C1Rd/αGC-pulsed cells after 6 h and 13 h stimulation (n = 3). Data on three individual animals shown. See also Figure S2

NKTT320 predominantly contained a mix of $CD4^+$ or $CD4^+CD8^+$ double-positive iNKT with few $CD8^+$ iNKT (data not shown).

We also used the degranulation flow cytometry experiment with *ex vivo* PBMC from three animals described earlier (Figure 2C) to measure apoptosis of co-cultured αGC-pulsed C1Rd cells in the absence or presence of NKTT320 (Figure 3B). Intracellular expression of activated Caspase-3 was used as an apoptosis marker. C1Rd cells were identified as $CD45^-HLA\text{-}DR^{hi}$ expressing live cells in the co-cultures (Figure S3C). Similar to our findings with expanded iNKT cultured cells, αGC stimulation of PBMC from all three

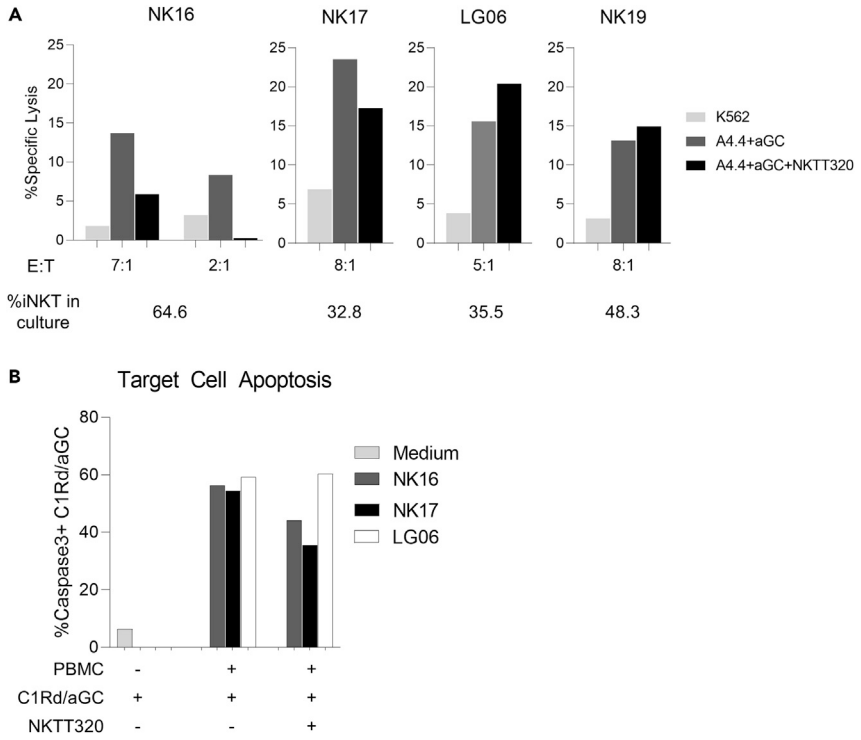

Figure 3. Killing capacity of NKTT320 activated iNKT

(A) Variable inhibition of specific lysis of αGC-pulsed CD1d-transfected K562 target cells (A4.4) in the absence or presence of NKTT320 (n = 4). Untransfected K562 targets used as controls. Effectors were iNKT expanded in culture for 10 days by stimulation with IL-2 and autologous irradiated PBMC pulsed with αGC. Effector to target (E:T) cell ratio and NKT frequency in culture are shown.

(B) Target cell apoptosis of CD1d-expressing C1R cells (C1Rd) loaded with αGC as measured by activated Caspase-3 expression after 6 h co-culture with PBMC of 3 MCM (NK16, NK17, LG06). In the NKTT320+αGC condition for both A and B, target cells (NKT lines or PBMC) were pre-incubated with NKTT320 followed by addition to αGC-pulsed targets to assess any inhibitory effects of NKTT320 on CD1d target cell recognition and killing. See also Figure S3

animals led to apoptosis of co-cultured αGC-pulsed C1Rd cells; however, apoptosis inhibition in the presence of NKTT320 was only seen in two of three animals (Figure 3B). Interestingly, these were the same two animals that displayed inhibition of killing in the presence of NKTT320 in the calcein release assay.

We also evaluated activation of putative CD1d-expressing antigen-presenting cells in this experiment. By gating on $CD45^{+}CD3^{-}CD8^{-}HLA\text{-}DR^{hi}$ live leukocytes, a population that would include B-cells, monocytes and DCs, we observed a variable increase in activated CD69-positive cells within this subset after NKTT320 stimulation in all three animals (Figure S3D). Activation was also seen after stimulation with αGC-pulsed C1Rd cells; pre-incubation with NKTT320 led to an enhanced effect in one animal LG06 but decrease in the other two animals NK16 and NK17 (Figure S3D). Although these data suggest the NKTT320-activated iNKT are able to activate antigen-presenting cells, they do not allow us to parse out cytokine-induced indirect effects from direct engagement via iNKT TCR/CD1d interaction.

In all these data indicate that NKTT320 can have a variable inhibitory effect on iNKT recognition of CD1d-expressing target cells. The biological significance of this effect and its comparison to αGC will require future *in vivo* experiments in different therapeutic settings.

NKTT320 pharmacokinetics

After determining the effectiveness and specificity of iNKT activation with NKTT320 *in vitro*, we set out to determine the pharmacokinetics of this antibody following *in vivo* administration. Dose escalation experiments were performed in three groups of MCM administered a single IV dose of NKTT320 at low (100 μg/kg, n = 5), mid (300 μg/kg, n = 3) and high (1000 μg/kg, n = 3) concentrations. These doses were selected

based on previously published data of NKTT120 (Scheuplein et al., 2013; Field et al., 2017). No adverse effects were observed following *in vivo* NKTT320 administration. Serum AST and ALT levels were transiently elevated one day after NKTT320 administration (Figure S4). Based on historical control values in normal cynomolgus macaques housed at the Tulane National Primate Research Center, serum ALT levels did not fall out of normal reference ranges. Mean AST levels were above the normal reference range at day 1 but returned within normal levels by day 3. Peak serum NKTT320 levels ranging between 5.94 and 77.46 μg/mL were reached within 24 h of a single IV dose (Figure S5A). The iNKT TCR saturation level previously determined for NKTT120 on a Biacore assay against the immobilized iNKT TCR resulted in a K_D of 44nm corresponding to a saturation level of 6 μg/mL (Scheuplein et al., 2013). All NKTT320-treated animals in the high- and mid-dosing groups reached peak levels above the NKT TCR saturation level (6 μg/mL) within 30 min of antibody administration while four of five animals in the low dose (100 μg/kg) surpassed TCR saturation levels within 2 h of administration (Figure S5A).

The kinetics of circulating NKTT320 showed animal to animal variation. Peak NKTT320 serum levels trended higher in the high dose group but did not reach significance (Figure S5A and data not shown). Plasma NKTT320 levels declined below detection in all animals 2–6 weeks after treatment, excepting one animal in the high dose group that maintained detectable serum NKTT320 levels through week 14. NKTT320 plasma concentrations in the high dose group were used to determine the half-life of NKTT320 (Figure S5B). The calculated half-life of 6.81 days or 163.2 h after administration is less than the half-life of NKTT120 but consistent with variation in plasma clearance of human IgG antibodies in NHPs (Scheuplein et al., 2013; Newman et al., 2001).

One multiply dosed animal with successive NKTT320 doses administered at two-week intervals (dose 1 = 30 μg/kg, dose 2 = 100 μg/kg and dose 3 = 100 μg/kg) reached the 6 μg/mL NKT TCR saturation level only after the second and third dose indicating that the first dose was not sufficient to surpass TCR saturation (data not shown). Multiple doses were additive in this animal and again peaked within 24 h after each administration (data not shown). These limited data suggest that doses above 30 μg/kg NKTT320 are needed for TCR saturation.

NKTT320 effect on iNKT after *in vivo* administration

We monitored *in vivo* changes in iNKT and non-iNKT ($V\alpha24^-$) T-lymphocytes from 30 min onwards following a single intravenous dose of NKTT320 (Figures 4A, 4B, S5C, and S5D). Similar to *in vitro* stimulation (Figures 1A–1D), *in vivo* NKTT320 resulted in downregulation of Vα24 TCR and CD1dTM-positive iNKT-cells within 24 h of administration (Figure S5C). Because NKTT320 binds to the invariant region of the NKT TCR, the decrease in CD1dTM-positive iNKT could represent a 'masking' effect. However, the attendant downregulation of Vα24 TCR and CD3 (data not shown) indicates that the decline in detectable Vα24/CD1dTM co-expressing iNKT following NKTT320 administration was also a result of *in vivo* NKT activation. Because of the loss of visualization of $V\alpha24^+CD1dTM^+$ iNKT we also enumerated total $V\alpha24^+$ T-lymphocytes to monitor changes in circulating iNKT frequency after NKTT320 administration (Figure S5D).

Both Vα24/CD1dTM co-staining iNKT and total $V\alpha24^+$ T-lymphocyte frequencies declined significantly after NKTT320 administration (Figure S5D). While Vα24/CD1dTM co-staining iNKT frequency was reduced by day 1 and remained significantly lower than baseline through week 14 ($p < 0.05$ at all sampled time-points), a significant decline in total $V\alpha24^+$ T-lymphocyte frequency was only observed for one week after NKTT320 administration. The decline in $V\alpha24^+CD1dTM^+$ iNKT, likely the result of a masking effect, persisted well beyond the time that serum NKTT320 levels were undetectable. This may mean that iNKT-bound NKTT320 undetectable in the blood is slowly released in the tissues and continues to activate iNKT.

Monitoring of HLA-DR and CD69 surface expression revealed rapid, sustained iNKT-specific activation without general T-lymphocyte activation following NKTT320 administration (Figure 4A). By 30 min, iNKT were significantly activated above baseline levels ($p = 0.0156$) while non-iNKT ($V\alpha24^-$) T-lymphocytes were not activated. iNKT then remained significantly activated for 6 weeks after treatment. Non-iNKT T-lymphocytes showed a transient significant increase in HLA-DR or CD69 expression after NKTT320 treatment. Activation levels of circulating iNKT remained significantly above non-iNKT T-lymphocytes starting within 30 min of NKTT320 administration ($p = 0.0039$) and persisted for at least 14 weeks ($p = 0.0391$).

To distinguish responses of iNKT subsets, we investigated differences in $CD8^-$ and $CD8^+$ iNKT activation. Both subsets were significantly activated within 30 min of NKTT320 administration; while $CD8^-$ iNKT

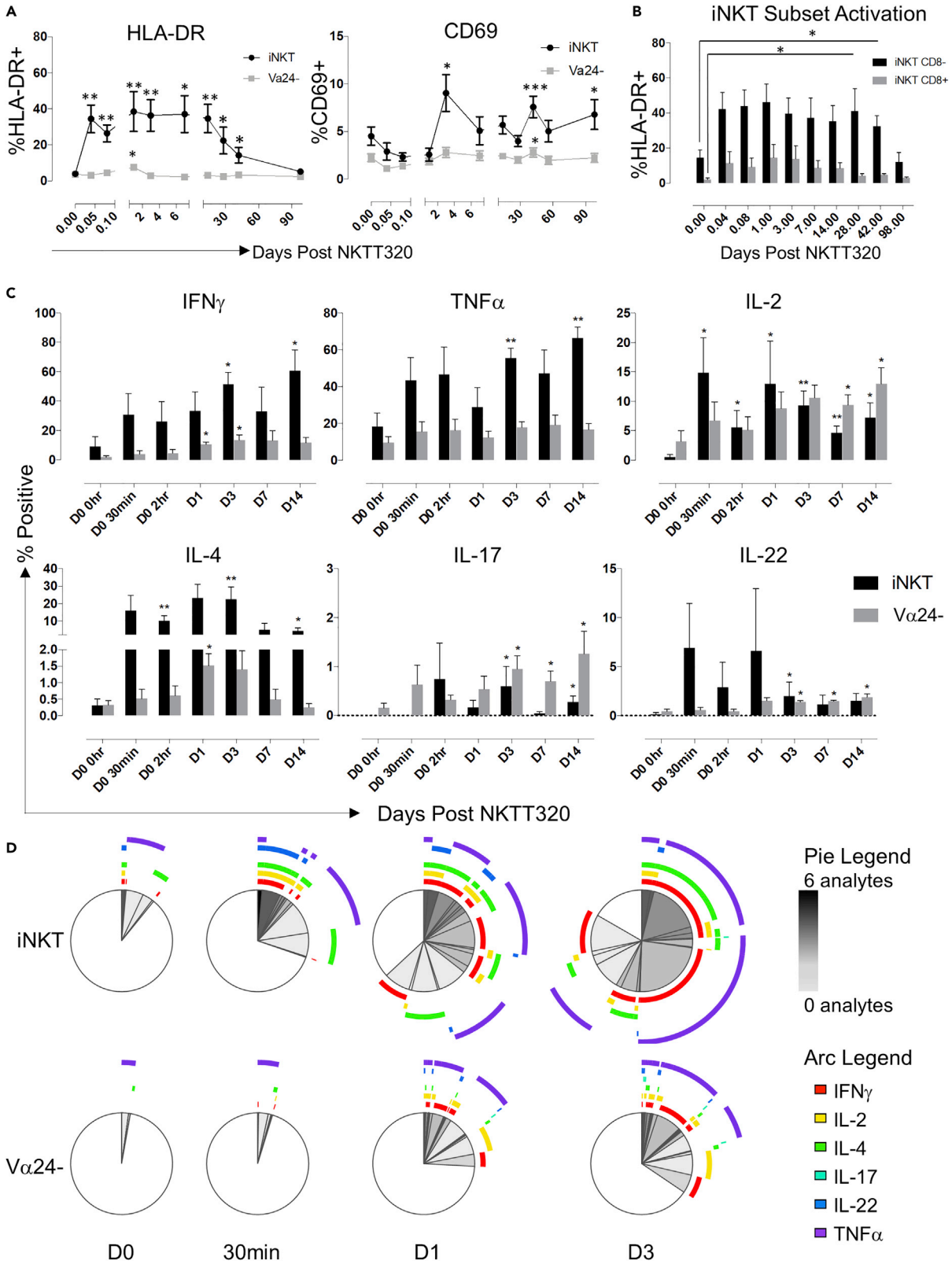
A
HLA-DR
%HLA-DR+
iNKT
Va24-
CD69
%CD69+
Days Post NKTT320
B
iNKT Subset Activation
%HLA-DR+
iNKT CD8-
iNKT CD8+
Days Post NKTT320
C
IFNγ
TNFα
IL-2
IL-4
IL-17
IL-22
% Positive
iNKT
Vα24-
Days Post NKTT320
D
iNKT
Vα24-
D0
30min
D1
D3
Pie Legend
6 analytes
0 analytes
Arc Legend
IFNγ
IL-2
IL-4
IL-17
IL-22
TNFα

Figure 4. *In vivo* iNKT activation modulates functionality of T cellsubsets

(A) Mean HLA-DR and CD69 expression in iNKT versus non-iNKT-T. (B) iNKT $CD8^-$vs iNKT $CD8^+$ in animals treated *in vivo* with NKTT320 (n = 9). Error bars show SEM.

(B) Paired t tests were used to determine statistical significance of increased activation of total iNKT or Va24- T (A), and $CD8^+$ or $CD8^-$iNKT (B) compared to their respective baseline values. * <0.05. Error bars show SEM.

(C) Mean cytokine expression in iNKTs and Non-iNKT Ts measured by intracellular cytokine staining following overnight PMA/ionomycin stimulation. Samples were taken at day 0 and 30 min, 2 h, day 1, 4, 7, 14. Data in n = 4 MCM. Significance compared to baseline is indicated by an asterisk and was determined by paired parametric t test. *<0.05, **<0.01. Error bars show SEM.

(D) SPICE analysis of iNKT vs Non-iNKT T cells indicating cytokine co-expression after stimulation with PMA/ionomycin (n = 4). See also Figures S4–S6

remained significantly activated through week six after treatment, increased $CD8^+$ iNKT activation lasted two weeks (Figure 4B). In contrast to *in vitro* data, circulating $CD8^-$ iNKT were significantly more activated compared to $CD8^+$ iNKT pre- and after NKTT320 administration ($p < 0.01$).

NKTT320 rapidly modulates T-lymphocyte function

Central to investigation of NKTT320's utility as an adjuvant is its effect on other immune cell subsets. We used intracellular cytokine staining (ICS) flow cytometry to evaluate NKTT320-induced functional changes in mitogen responsiveness of iNKT and non-iNKT T-lymphocytes at discrete time-points after IV NKTT320 administration. Increased responsiveness of iNKT to overnight PMA/ionomycin stimulation was observed within 30 min of NKTT320 administration (Figures 4C and 4D). A significant increase in IL-2 secretion detected at 30 min after NKTT320 was sustained through day 14 after treatment. Likewise, IL-4 was significantly upregulated within 2 h of NKTT320 treatment. Significant increases in IFNγ and TNFα were observed day 3 onwards. Increased responsiveness to mitogen stimulation was also observed in $V\alpha24^-$ "non-iNKT" T-lymphocytes but at a later onset suggesting downstream activation of other T-lymphocyte subsets. The increase in cytokine production in both iNKT and non-NKT T-lymphocytes mainly originated from $CD4^+$ T lymphocytes (Figure S6A and data not shown).

NKTT320 also rapidly increased iNKT polyfunctionality; by day 1, over 50% of responding iNKT secreted two or more cytokines on mitogen stimulation (Figures 4D and S6B). Despite TCR downregulation, a discernable iNKT population was visible at early time-points after NKTT320 administration in most animals to allow evaluation of its function by flow cytometry (Figure S6C). Increased polyfunctionality was less evident in the non-NKT T-lymphocytes. Overall, iNKT were activated rapidly in response to NKTT320 treatment and appear to have also induced changes in the functional potential of non-iNKT T-lymphocytes.

In vivo iNKT activation results in rapid activation of the innate and adaptive immune system

The ability to modulate innate and adaptive immune responses is crucial when identifying promising immune modulatory tools and vaccine adjuvants. To assess the effect on the host immune response we longitudinally measured plasma analytes by Luminex, and monitored changes in immune cell frequency, phenotype and function by flow cytometry after *in vivo* administration of NKTT320.

A significant increase in 21 plasma analytes was detected in the first 72 h of NKTT320 administration (Figure 5A, Table S1). Plasma CCL2, CXCL10 and IL-6 were elevated within 30 min reaching peak levels in the first 2 h (Figure 5B). Significantly elevated analytes that peaked in the first 24 h included cytokines and chemokines that likely originated from iNKT (IL-2, IL-4, IL-5, IL-6, IL-10, CCL4, CCL5) and from downstream activation of dendritic cells and monocytes/macrophages (IL-12, IL-1β, IL-1RA, CXCL8, CXCL9-11, IL-6, CCL2, CCL22). Interestingly, IFNγ, TNFα and GM-CSF peaked later at 72 h (Table S1) suggesting iNKT and non-iNKT sources such as NK cells and other T-lymphocytes. Of note, the increase in plasma analytes corresponded temporally to the peak of plasma NKTT320 and iNKT-specific activation. The early response was indicative of rapid activation of the innate immune system and included proinflammatory analytes as well as several chemo-attractants crucial for immune cell recruitment of monocytes, granulocytes, NK cells and activated T-lymphocytes (Bromley et al., 2008; Deshmane et al., 2009).

Consistent with the Luminex data, flow cytometry revealed significant changes in circulating monocytes and B-lymphocytes (Figures 5C and 5D). A significant increase in $CD14^+$ monocytes detected at day 1 after NKTT320 treatment had declined to baseline levels by week 6 (Figure 5C). Increased levels of proliferating $CD20^+$ B-lymphocytes as measured by Ki67 were detected beginning at day 1 ($p = 0.0156$) and intermittently thereafter (Figure 5D). These data are consistent with downstream effects of iNKT activation on other immune cell populations. The broad range of cytokines, chemokines and growth factors detected in

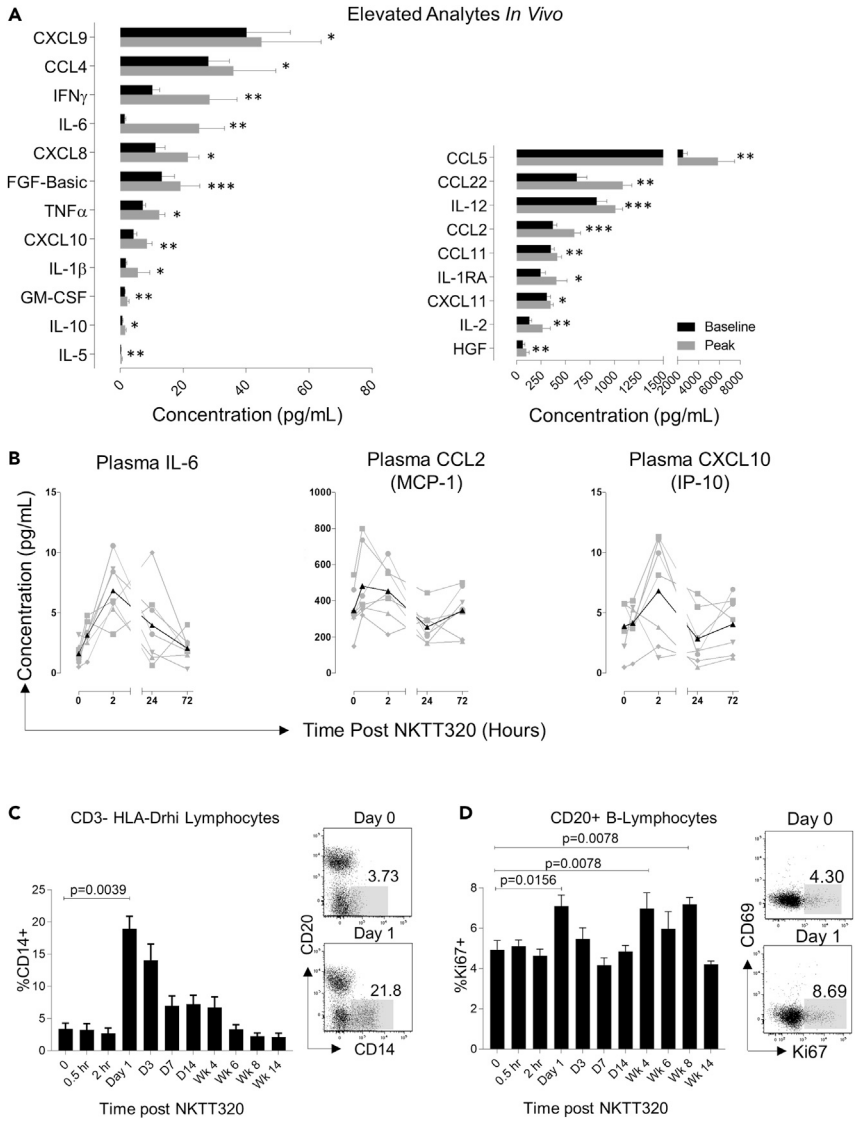

Figure 5. NKTT320 rapidly induces functional and bystander changes *in vivo*

(A) Analytes significantly upregulated after NKTT320 treatment *in vivo* measured by plasma Luminex at baseline and peak (n = 12). Mean and SEM are shown. *<0.05, **<0.01, ***<0.001.

(B) *Ex vivo* plasma Luminex kinetics after NKTT320 for IL-6, CCL2, and CXCL10 in seven animals from a single Luminex run.

(C) Monocyte frequency shown as percentage of $CD3^-$ HLA-DRhi lymphocytes. Representative plots show an increase in circulating monocytes on day 1 compared to day 0. Mean and SEM are shown.

(D) B-cell proliferation measured by Ki67 expression on $CD20^+$ B-cells. Representative plots show increases in B-cell Ki67 expression at day 1 after NKTT320 administration. Mean and SEM are shown. Significant differences from baseline were determined through non-parametric Wilcoxon signed-rank test (n = 9 MCM). See also Table S1

response to NKTT320 treatment underscores its ability to rapidly activate the innate immune system and potentially be an immunomodulatory tool.

RNA-seq analysis of effects of *in vivo* NKTT320

To further investigate host immune modulation by NKTT320, we performed bulk RNA-Seq analysis on frozen unfractionated PBMC collected at 0, 30 min, 2 h, and 24 h time-points after NKTT320 administration in four MCM with iNKT frequencies ranging between 0.018 and 9.56% of circulating T-lymphocytes (Figures 6, 7, and S7). RNA-Seq analysis revealed significant sequential differential gene expression following

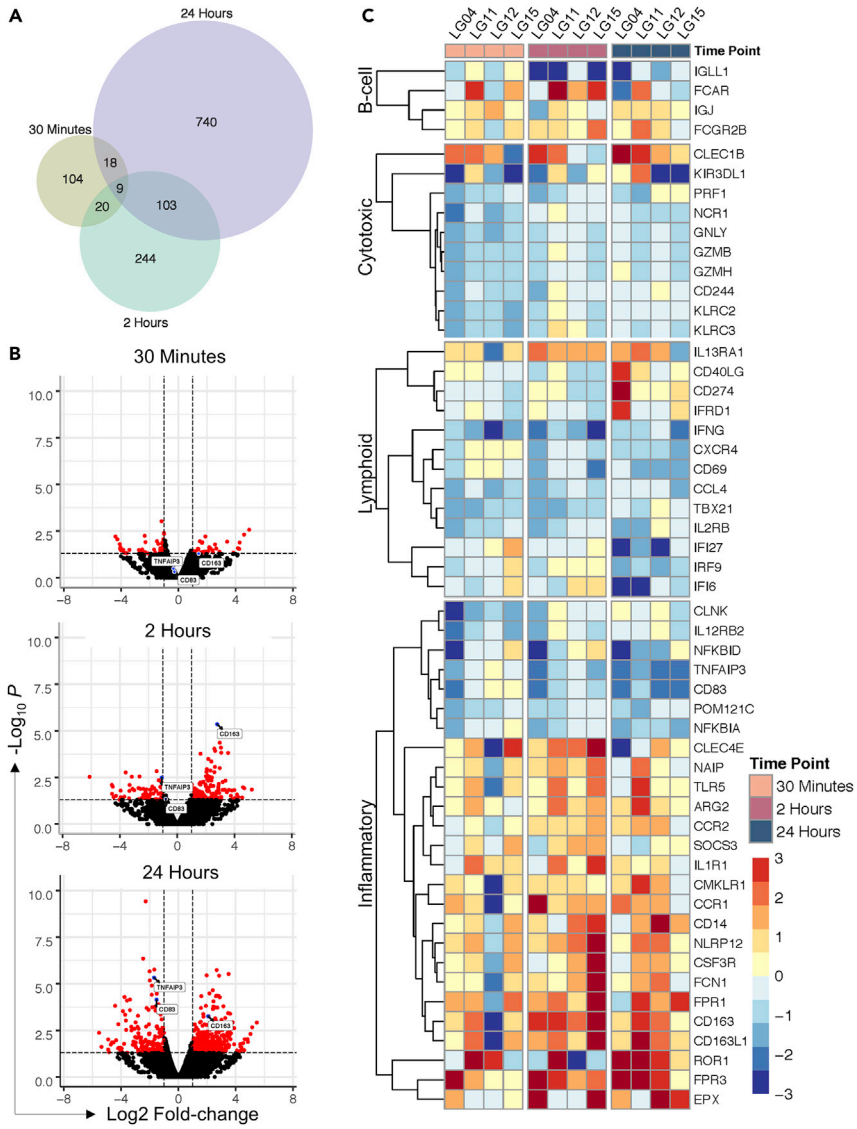

Figure 6. RNA-seq analysis reveals rapid differential gene expression

(A) Venn diagram showing differentially expressed genes where p value <0.05 at 30 min, 2 h and 24 h.

(B) Volcano plots of all genes showing kinetic increases in transcriptomic changes over time.

(C) Heatmaps showing differential expression (log_2 fold change) for targeted genes where p value <0.05 related to B-cell, cytotoxic, lymphoid and inflammatory pathways. See also Figure S7 and Table S2

NKTT320 treatment. At 30 min after NKTT320, there were 104 unique genes differentially expressed, followed by 244 and 740 genes at 2 and 24 h, respectively (Figure 6A, Table S2). Volcano plots showed significant changes in several genes. Notably, the scavenger receptor CD163 exclusively expressed on monocytes and macrophages (Moestrup and Moller, 2004), was significantly upregulated as early as 30 min and sustained through 24 h (Figures 6B and 6C). Concomitantly, CD83 and TNF-Alpha-Induced Protein 3 (TNFAIP3) were significantly downregulated at 24 h (Figure 6B). CD83, a member of the immunoglobulin (Ig) superfamily expressed on mature DCs can regulate inflammation by suppressing IL-12 and MCP-1 production (Bates et al., 2015). Downregulation of TNFAIP3 or A20, an inhibitor of TCR signaling and NF-κB activation (Das et al., 2018) was consistent with promotion of an inflammatory response.

Targeted analysis of differentially expressed genes showed elevation of several lymphoid genes related to monocytes, granulocytes, B-cells, T-cells and NK-cells as early as 30 min after NKTT320 administration

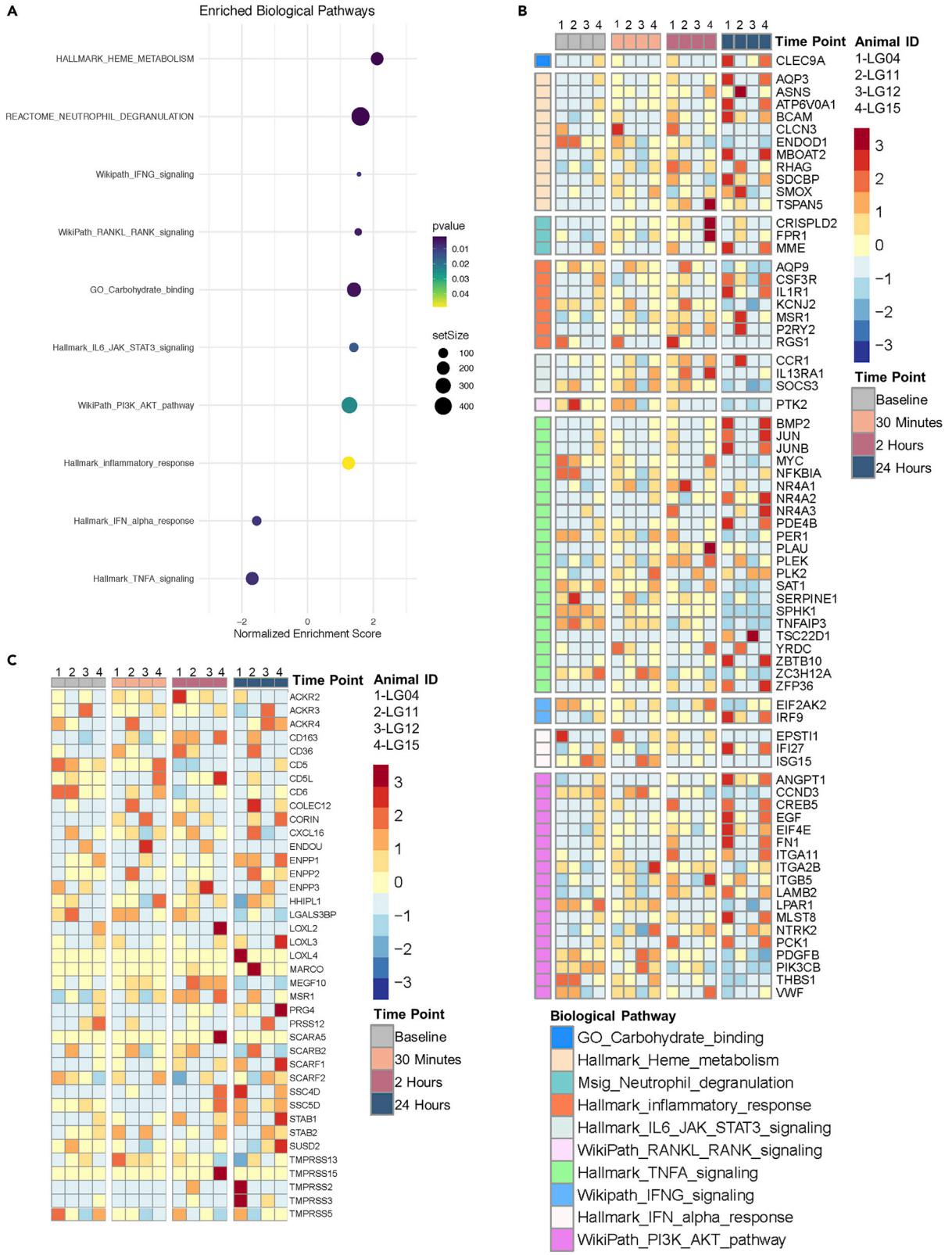
A
Enriched Biological Pathways
HALLMARK_HEME_METABOLISM
REACTOME_NEUTROPHIL_DEGRANULATION
Wikipath_IFNG_signaling
WikiPath_RANKL_RANK_signaling
GO_Carbohydrate_binding
Hallmark_IL6_JAK_STAT3_signaling
WikiPath_PI3K_AKT_pathway
Hallmark_inflammatory_response
Hallmark_IFN_alpha_response
Hallmark_TNFA_signaling
−2
0
2
Normalized Enrichment Score
pvalue
0.01
0.02
0.03
0.04
setSize
100
200
300
400
B
1 2 3 4 1 2 3 4 1 2 3 4 1 2 3 4
Time Point
Animal ID
1-LG04
2-LG11
3-LG12
4-LG15
CLEC9A
AQP3
ASNS
ATP6V0A1
BCAM
CLCN3
ENDOD1
MBOAT2
RHAG
SDCBP
SMOX
TSPAN5
CRISPLD2
FPR1
MME
AQP9
CSF3R
IL1R1
KCNJ2
MSR1
P2RY2
RGS1
CCR1
IL13RA1
SOCS3
PTK2
BMP2
JUN
JUNB
MYC
NFKBIA
NR4A1
NR4A2
NR4A3
PDE4B
PER1
PLAU
PLEK
PLK2
SAT1
SERPINE1
SPHK1
TNFAIP3
TSC22D1
YRDC
ZBTB10
ZC3H12A
ZFP36
EIF2AK2
IRF9
EPSTI1
IFI27
ISG15
ANGPT1
CCND3
CREB5
EGF
EIF4E
FN1
ITGA11
ITGA2B
ITGB5
LAMB2
LPAR1
MLST8
NTRK2
PCK1
PDGFB
PIK3CB
THBS1
VWF
3
2
1
0
−1
−2
−3
Time Point
Baseline
30 Minutes
2 Hours
24 Hours
Biological Pathway
GO_Carbohydrate_binding
Hallmark_Heme_metabolism
Msig_Neutrophil_degranulation
Hallmark_inflammatory_response
Hallmark_IL6_JAK_STAT3_signaling
WikiPath_RANKL_RANK_signaling
Hallmark_TNFA_signaling
Wikipath_IFNG_signaling
Hallmark_IFN_alpha_response
WikiPath_PI3K_AKT_pathway
C
1 2 3 4 1 2 3 4 1 2 3 4 1 2 3 4
Time Point
Animal ID
1-LG04
2-LG11
3-LG12
4-LG15
ACKR2
ACKR3
ACKR4
CD163
CD36
CD5
CD5L
CD6
COLEC12
CORIN
CXCL16
ENDOU
ENPP1
ENPP2
ENPP3
HHIPL1
LGALS3BP
LOXL2
LOXL3
LOXL4
MARCO
MEGF10
MSR1
PRG4
PRSS12
SCARA5
SCARB2
SCARF1
SCARF2
SSC4D
SSC5D
STAB1
STAB2
SUSD2
TMPRSS13
TMPRSS15
TMPRSS2
TMPRSS3
TMPRSS5
3
2
1
0
−1
−2
−3
Time Point
Baseline
30 Minutes
2 Hours
24 Hours

Figure 7. Biological pathways related to NKT cells are enriched upon anti-NKT antibody administration

(A). Normalized enrichment scores (NES) of relevant NKT-related pathways selected from an unbiased gene set enrichment analysis (GSEA). Color ramp represents NES significance defined by a Fisher Exact test. Dot size represents 'setSize', or number of genes contained within an *a priori*-defined biological pathway.

(B) Composite heatmap of genes meeting a significance threshold ($p < 0.05$) at 30 min-, 2 h-, and 1 day after NKT-antibody administration that are contained within significantly enriched pathways depicted in (A). Rows are scaled by z-score-normalized expression.

(C) Heatmap of genes within the GO pathway "scavenger receptor activity". See also Figure S7, Tables S3, and S4

(Figure 6C). Notable among these were upregulation of the following genes: the low affinity inhibitory Fc gamma receptor FCGR2B involved in regulation of antibody production by B-cells and modulation of antibody-dependent effector function of myeloid cells (Nimmerjahn and Ravetch, 2008); Fc fragment of IgA receptor FCAR present on myeloid lineage cells and mediating phagocytosis and ADCC (Monteiro and Van de Winkel, 2003); C-type lectin-like receptor CLEC1B expressed on NK cells (Huysamen and Brown, 2009); CD14, CD163 expressed on monocytes and macrophages; IL-13 receptor alpha-1 chain (IL13RA1) involved in activation of JAK1, STAT3 and STAT6 induced by IL13 and IL4 (McCormick and Heller, 2015); the MCP-1 receptor CCR2 mediating monocyte chemotaxis (Deshmane et al., 2009); CD40 ligand (CD40L) expressed on iNKT and T-cells promoting DC-iNKT interactions and regulating B-cell function through CD4 help (Brennan et al., 2013); colony stimulating factor 3 (CSF3R) or G-CSF receptor controlling granulocyte maturation and function (Ward, 2007); and N-formyl peptide receptors (FPR1, FPR3) that are powerful neutrophil chemotactic factors (Dahlgren et al., 2020). Several inflammation-related and pattern-recognition receptor genes were elevated. These included IL1R1; extracellular and cytosolic receptors for bacterial flagellin, namely toll-like receptor 5 (TLR5), and neuronal apoptosis inhibitory protein NAIP that also acts as the sensor component of the NLRC4 inflammasome and promotes caspase-1 activation (Zhao and Shao, 2015); the carbohydrate sensing innate immune recognition ficolin FCN1 expressed in monocytes (Gout et al., 2010); and the C-type lectin receptor CLEC4E or MINCLE expressed on macrophages that recognizes fungal and mycobacterial ligands (Furukawa et al., 2013). Upregulation of the chemokine receptor genes CCR2 and CCR1 was concordant with elevated plasma levels of their respective ligands, CCL2 and MIP-1α, after NKTT320 administration (Figure 6 and Table S1). Overall, upregulation of these genes was indicative of a broad stimulation of the innate immune system with facilitation of antigen presentation function.

Simultaneously an immune downmodulation effect of NKTT320 was evident by upregulation of several immune inhibitory and inflammation suppressive genes (Figure 6). These included the T-lymphocyte inhibitor PD-1 ligand 1 (CD274) (Freeman et al., 2000); the arginine metabolism enzyme ARG2 that can regulate inflammation and immunity (Asosingh et al., 2020; McGovern et al., 2017; Geiger et al., 2016; Dowling et al., 2021); the potent mitigator of inflammation, nucleotide-binding oligomerization domain protein NLRP12 that acts as a negative regulator of NF-κB and promotes degradation of NOD (Normand et al., 2018); the chemerin chemokine-like receptor CMKLR1 which binds the endogenous lipid mediator Resolvin E1 and actively regulates resolution of acute inflammation (Ohira et al., 2010), the suppressor of cytokine signaling SOCS3 involved in the negative regulation of cytokines such as IL6 that signal through the JAK/STAT pathway (Heinrich et al., 1998), and ROR1 that can inhibit the Wnt3a-mediated signaling pathway (Bainbridge et al., 2014). These data point to an inflammation suppressive effect of NKTT320-mediated iNKT activation acting in concert with activation of B-cells, monocytes, dendritic cells, and T-helper pathways. It is noteworthy that both activating and suppressive effects were detected in the first 24 h of NKTT320 administration. The inhibitory signals may reflect a feedback loop following initial activation.

Downregulation of genes such as PRF1, NCR1, GNLY, GZMB, GZMH, CD244 associated with T-lymphocyte and NK cytotoxicity (Figure 6) was unexpected due to the functional evidence for T-lymphocyte activation. Of these, CD244 or 2B4, which belongs to the signaling lymphocyte activation molecule (SLAM)-receptor family and is expressed on NK cells, as well as on some T cells, monocytes and basophils, can serve as both an activating and inhibitory receptor (Eissmann et al., 2005).

We followed the targeted gene analysis with an unbiased analysis of differentially expressed genes after NKTT320 administration (Figure 7). Using Gene Set Enrichment Analysis against four pathway databases, an aggregate of 201, 332, and 423 enriched pathways were detected at 30 min, 2 and 24 h respectively after NKTT320 administration (Tables S3 and S4). Normalized enrichment scores of 10 biological pathways related to NKT-lymphocytes that were significantly altered on NKTT320 administration along with heatmaps of genes in these pathways reaching a significant threshold are shown (Figures 7A and 7B). Because

of CD163 upregulation and upregulation of genes involved in phagocytosis we also evaluated genes in the scavenger receptor activity pathway (Figure 7C).

Several genes from the inflammatory response, heme metabolism, neutrophil degranulation, IL-6/JAK/STAT3, and PI3K/AKT pathways were increased within 24 h of NKTT320 (Figure 7B). Among the upregulated genes, elevation of the CLEC9A gene in the carbohydrate binding pathway was noteworthy. Targeting antigens to the C-type lectin CLEC9A on DCs can induce strong humoral immunity and T follicular helper responses independent of adjuvant and is being explored as a vaccine strategy (Caminschi et al., 2008; Cueto et al., 2019). Upregulation of the heme metabolism pathway SDCBP gene encoding the syndecan binding protein or syntenin-1 is interesting as it regulates TGFβ1-mediated downstream activation (Hwangbo et al., 2016).

Downregulated genes in the pathway analysis included the cyclin family gene CCND3, platelet-derived growth factor PDGFB, PIK3CB, and LPAR1, a member of the G protein-coupled receptor superfamily with diverse biological functions including proliferation and chemotaxis. The functional effects of genes that were downregulated appeared to be both pro-activation as well as anti-inflammatory. Several of the downregulated genes in the TNFA signaling pathway were inhibitors of NF-κB activation and it is likely that their suppression would lead to increased activation. Examples include suppression of TNFAIP3 and ZC3H12A, an IL-1-inducible gene encoding the monocyte chemotactic protein-1-induced protein-1 (MCPIP1), that acts as a transcriptional activator but also suppresses NF-κB activation (Jura et al., 2012). Similarly, suppression of the sphingosine kinase one gene (SPHK1) has been shown to potentiate induction of RANTES (Adada et al., 2013). The clock gene PER1 regulates proinflammatory mediators, and its suppression can lead to increased CCL2 and IL6 (Sugimoto et al., 2014). On the other hand, downregulation of PIK3CB or PI-3 kinase subunit beta in the PI3K/AKT pathway can be instrumental in suppressing inflammation by prevention of AKT phosphorylation and inducing FOXO activation (Finlay and Cantrell, 2011).

iNKT maintain proliferative ability and avoid anergy following NKTT320 treatment

One hurdle to therapeutic modalities of *in vivo* iNKT activation from data in mice is the induction of iNKT anergy. Administration of soluble αGC *in vivo* results in rapid iNKT activation followed by subsequent iNKT anergy in response to further stimulation (Parekh et al., 2005). To test whether *in vivo* NKTT320 treatment induces anergy in macaques, we performed *in vitro* proliferation assays in PBMC from NKTT320-treated animals, measuring Ki67 and BrdU double-positive cells after a 6-day stimulation with αGC. iNKT of animals that had received NKTT320 did not display anergy. On the contrary they were more responsive to *in vitro* αGC stimulation and showed increased proliferation compared to a pre-NKTT320 time-point (Figure S8A). Furthermore, iNKT-cells continued to expand in culture on αGC stimulation pre- and after NKTT320 treatment providing further evidence that the monoclonal antibody does not induce iNKT anergy (Figure S8B). The increased *in vitro* iNKT expansion was specific to αGC stimulation and not seen with other stimuli (Figure S8B). These results were reproducible at day 1 after NKTT320 in three of five animals assessed by proliferation assays (data not shown). We saw a comparable or greater increase in plasma IL1RA, IL-6 and MCP-1 after a second dose of NKTT320, providing further evidence for absence of anergy (Figure 8A). In one multiply dosed animal, iNKT proliferative ability temporally followed increases in NKTT320 plasma concentration after each dose (Figure 8B).

Increased iNKT response in adipose tissue after NKTT320 administration

Our observations on the effect of NKTT320 were thus far confined to the examination of peripheral blood where we did not detect an increase in iNKT frequency. To investigate trafficking or effect on tissue iNKT, we examined iNKT frequency pre-and 14 days after NKTT320 administration in lymph node (LN), bone marrow (BM), bronchoalveolar lavage (BAL), rectal mucosa (REC) and adipose tissue in a subset of animals. Adipose tissue is known to be a site of iNKT localization in humans (Lynch, 2014). Interestingly, we observed an increased frequency of adipose iNKT after NKTT320 treatment while iNKT frequency at other tissue sites was unchanged (Figures 8C and 8D). This suggests that either adipose-resident iNKT proliferate in response to NKTT320 treatment or iNKT are trafficking to adipose tissue following NKTT320 treatment. Further studies such as direct assessment of adipose iNKT for expression of Ki67 are needed to determine whether iNKT proliferate locally in response to NKTT320 treatment.

In preliminary studies, we were able to compare the cytokine-secreting function of mitogen-stimulated adipose and PBMC iNKT by flow cytometry at pre- and after NKTT320 treatment time-points in n = 4 and n = 2 animals, respectively. Adipose iNKT were distinct from PBMC iNKT in having higher frequencies of

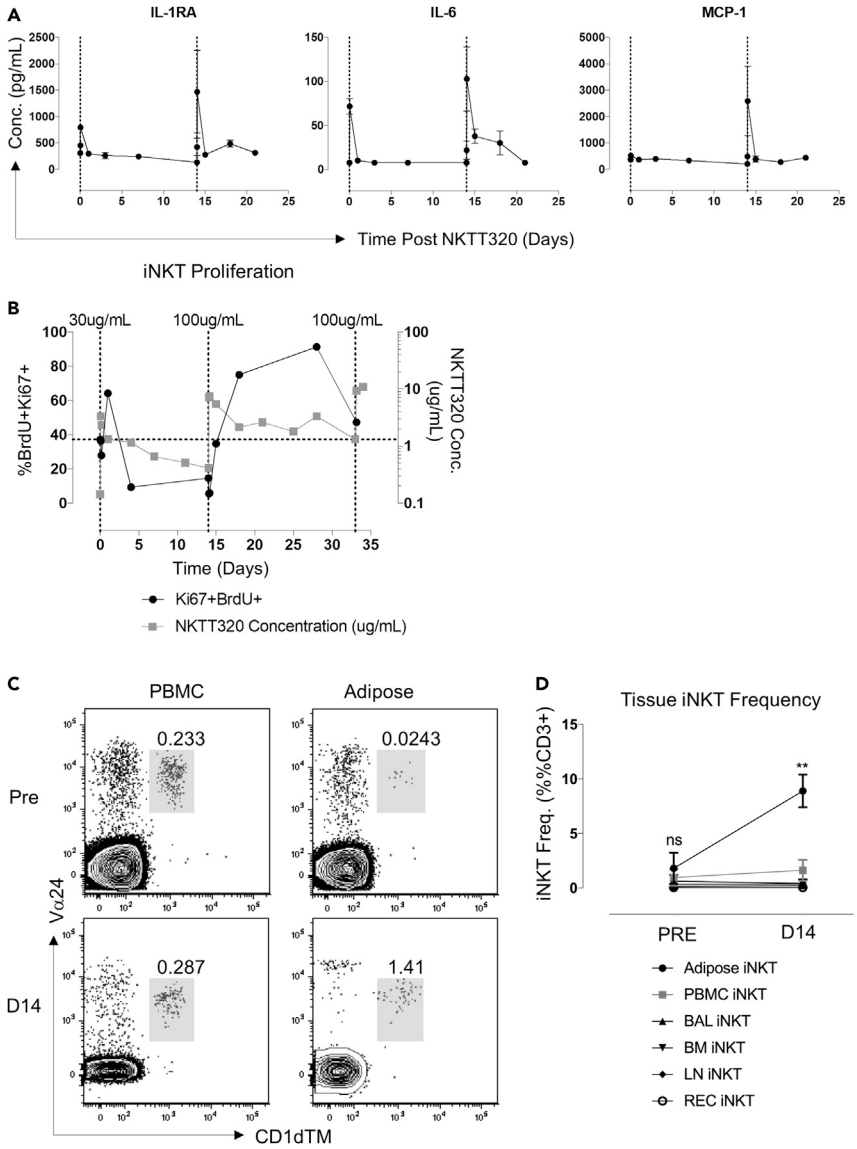

Figure 8. iNKTs retain proliferative capacity and traffic to adipose tissue after NKTT320 indicating a lack of NKT anergy

(A) *Ex vivo* plasma luminex data from animals that received 2 doses of NKTT320 (n = 4). Mean and SEM shown.

(B) iNKT proliferation measured as BrdU + Ki67 + double-positives by flow cytometry. Proliferation data is compared to plasma NKTT320 concentration measured by NKTT320 ELISA. Vertical lines indicate the time and concentration of each dose. Horizontal line indicates baseline iNKT proliferation. Vertical lines indicate timing of dosing. Data in one multiply dosed MCM.

(C) Representative plots of iNKT frequency pre and post NKTT320 treatment in white adipose and PBMC.

(D) iNKT frequency in tissues and PBMC pre and 14 days after NKTT320 treatment (n = 3). Paired t test, **<0.01. 'PBMC-peripheral blood mononuclear cells; 'BAL'-bronchoalveolar lavage; 'BM'-bone marrow; 'LN'-lymph node; 'REC'-rectal mucosa. Mean and SEM is shown. See also Figures S8 and S9

IL-2- and IL-4-secreting cells (Figure S9A). Adipose iNKT were also more polyfunctional compared to PBMC iNKT with over 30% of cells secreting three or more cytokines compared to less than 5% of PBMC iNKT (Figure S9A). These differences continued to be observed at two weeks after NKTT320 treatment (Figure S9B) suggesting that iNKT in the adipose are distinct from circulating iNKT. However, because these data are both preliminary and limited, further studies are needed to conclusively define differences in adipose and PBMC iNKT in the context of NKTT320.

DISCUSSION

This study is the first demonstration of sustained *in vivo* iNKT activation using the iNKT-activating humanized monoclonal antibody, NKTT320, that selectively binds with high affinity to the invariant NKT TCR in humans (Patel et al., 2020). We used the non-human primate model of MCM to extensively characterize the *in vitro* and *in vivo* effects of NKTT320 and assess its utility as an immunomodulatory tool. *In vitro*, NKTT320 showed dose-dependent iNKT-specific activation and increased cytokine production. *In vivo*, a single intravenous inoculation of NKTT320 was sufficient to rapidly induce iNKT activation that was sustained for up to 6 weeks without causing anergy. *In vivo* NKTT320-induced iNKT activation was associated with downstream activation of non-NKT immune cell subsets and iNKT trafficking to or proliferation within adipose tissue. Even though iNKT accounted for only 0.018–10.4% of circulating T-lymphocytes at baseline, iNKT activation had a profound amplification effect because of downstream effects on a wide range of immune cells. Our findings on *in vivo* iNKT activation and downstream effects on $CD4^+$ T-lymphocytes, monocytes, dendritic cells and B cells, make NKTT320 a promising candidate for immunotherapy with translational potential.

In vivo NKTT320 administration led to iNKT-specific activation within 30 min of administration and was accompanied by increased iNKT polyfunctionality with Th1 and Th2 cytokine secretion, increased proliferative capacity and increased adipose tissue iNKT. A greater stimulatory effect on $CD4^+$ iNKT was observed as they were the major source of the cytokines contributing to increased polyfunctionality in mitogen-stimulated iNKT. An increase in IL-2 and IL-4 was followed by IFNγ and TNFα production. IL-2 and IL-4 are both known to regulate and promote T cell differentiation into Th1 and Th2, respectively. In addition, lymph node iNKT secreting IL-4 were recently shown to be a key mediator of humoral immunity, improving B-cell maturation and differentiation as well as antibody class switching (Gaya et al., 2018; Lee et al., 2015). Early increases in iNKT function were followed from day 3 onwards by increased cytokine secretion from non-iNKT T-lymphocytes, most notably IL-2, IL-17 and IL-22. Induction of Th17/Th22 cytokines is of particular interest in the context of HIV infection as they are known to play a major role in maintaining gut mucosal integrity.

NKTT320-induced activation had features that were distinct from glycolipid iNKT agonists. While NKTT320 activated iNKT within 2 h of stimulation and reached peak response levels by 16 h, αGC stimulation was slower to catch up requiring 48 h to reach comparable levels. In addition, NKTT320 resulted in a broader Th1 and Th2 response without significant degranulation whereas αGC skewed toward Th1 and iNKT degranulation. Few *in vivo* studies of iNKT activation using αGC in humans and macaques have described functional changes by ICS in response to mitogen stimulation. When described, increases in Th1 cytokine production, primarily IFNγ were reported (Fernandez et al., 2013). Although synthetic sphingolipid NKT agonists that drive Th2 responses are available (Bricard et al., 2010), NKTT320 may be advantageous because it fosters an environment of increased responsiveness directing polyfunctional responses to specific stimuli without the need for structural modifications. Because NKTT320 binds to the iNKT TCR, it may affect the ability of activated iNKT to engage with CD1d-expressing antigen-presenting cells or tumor target cells. Indeed, our *in vitro* experiments showed a partial inhibitory effect of NKTT320 on iNKT killing of CD1d-expressing target cells in some animals. Whether this property would impact induction of antigen-specific $CD8^+$T cell responses remains to be determined. Future *in vivo* studies are needed to compare the relative efficacy of NKTT320 over sphingolipid agonists as a vaccine adjuvant or as an immunotherapeutic tool in anti-tumor therapy. Because NKTT320 does not rely on CD1d-mediated antigen presentation for iNKT activation, this could be an advantage in disease settings such as HIV infection associated with CD1d downregulation (Chen et al., 2006; Moll et al., 2010).

Circulating iNKT frequencies were transiently reduced after NKTT320, consistent with previous studies of *in vivo* iNKT activation using αGC in pig-tailed macaques and humans (Fernandez et al., 2013; Giaccone et al., 2002; Woltman et al., 2009). It is important to consider that the decrease in circulating iNKT frequency could be the result of a masking effect because of NKTT320 binding to the same site as CD1dTM, or to activation and subsequent downregulation of the iNKT TCR rendering it difficult to detect iNKT. Another explanation is that iNKT trafficking to tissue effector sites after activation could also transiently decrease the frequency of circulating iNKT. Our observation of elevated iNKT frequencies in adipose tissue following NKTT320 treatment suggests this possibility. This is an interesting finding as adipose tissue has been recently recognized as an inflammatory site with significant involvement in metabolic syndromes (Saltiel and Olefsky, 2017). In addition, adipose tissue is a known site of HIV/SIV reservoir (Damouche et al., 2015). iNKT are known HIV/SIV targets (Motsinger et al., 2002) and may be depleted early in infection rendering them less amenable to NKTT320-mediated manipulation of the adipose tissue HIV reservoir. Further investigation of the tissue effects of NKTT320 is warranted.

Because of the unique regulatory function of iNKT-cells, iNKT activation influences downstream immune cells. Through multiple lines of evidence based on flow cytometry, Luminex and RNA-Seq data, we show profound and broad effects of NKTT320 on the innate and adaptive immune system, particularly on monocytes/macrophages. Increased levels of plasma IL-6, CCL2 and CXCL10 were detected as early as 30 min after NKTT320 antibody administration. A significant increase in circulating $CD14^+$ monocyte frequency was observed at day 1 along with rapid upregulation of CD14, CD163 and CLEC4E gene expression within 30 min of antibody administration. In addition, CCR2 (present on activated macrophages) gene expression was significantly upregulated at 2 h in concert with significantly elevated plasma levels of its ligand CCL2. These data point to a rapid release of proinflammatory cytokines and chemokines along with mobilization of monocytes and activated macrophages initiated by NKTT320 administration. The downstream effects of NKTT320-mediated iNKT activation also included release of chemo-attractants involved in the recruitment of granulocytes, NK cells, and T-lymphocytes to sites of inflammation. Increase in chemokines involved in granulocyte recruitment included CCL11 (eotaxin) for eosinophil recruitment; CXCL8 (IL8) for neutrophil recruitment; CCL2 (MCP1) chemoattractant for basophils and monocytes; CXCL9-11 for chemoattraction of Th1 CXCR3-expressing T-cells to inflammatory sites; and CCL22 (MDC) chemoattractant for monocytes, DC, NK and T-lymphocytes (Bromley et al., 2008). Surprisingly, several genes in the IFNγ and TNFα signaling pathways and cytotoxic related genes were downregulated despite evidence of elevated plasma TNFα and IFNγ by Luminex. Although unexpected, the transcriptomics data represented a snapshot of the first 24 h whereas in the Luminex we saw plasma levels of TNF-α and IFN-γ peak only at 72 h. Moreover, mRNA and protein expression levels are often discordant for the same time-point during dynamic transitions, as was the case in the first 24 h of NKTT320 administration which likely explains differences in Luminex and RNA-Seq data (Liu et al., 2016).

Several pattern recognition receptor genes expressed on dendritic cells and monocyte/macrophages were modulated by NKTT320. Notable among them was the C-lectin type receptor CLEC9a which has been shown to efficiently induce humoral immunity and a T follicular helper response when used to present antigen to B-cells (Caminschi et al., 2008; Kato et al., 2015). In addition, TLR5, a ubiquitous pathogen recognition marker, and NAIP involved in bacterial flagellin recognition were upregulated. CD40 ligand (CD40L) gene expression was also upregulated likely on NKT and other $CD4^+$ T-lymphocytes. A major pathway by which NKT promote DC/APC maturation is by upregulation of CD40L providing co-stimulation to DCs via CD40L and IFNγ, TNFα (Brennan et al., 2013). NKT licensing of DCs for antigen cross-presentation can determine the type of the immune response. These data underscore the effect of NKTT320 on APCs which could lead to improved antigen presentation and potentiation of cellular immunity. *In vivo* NKTT320 treatment also had downstream effects on B-cells suggesting synergistic effects that likely improve humoral immunity. Definitive determination of the effect of *in vivo* NKTT320 treatment on modulating antigen-specific cellular and humoral immunity awaits future vaccine studies in the absence and presence of NKTT320.

Interestingly, our data show the potential of NKTT320 to modulate both inflammatory and anti-inflammatory responses. As illustrated in the schematic (Figure 9), side-by-side with activation, NKTT320 triggered several genes encoding markers of resolution of inflammation. Most prominent of the upregulated genes included the inflammation resolution genes NLRP12 and CMKLR1 (Fullerton and Gilroy, 2016; Ohira et al., 2010), the metabolic regulator ARG-2 (Dowling et al., 2021), and the inhibitory receptors FCGR2B and PD-L1 (Nimmerjahn and Ravetch, 2008; Freeman et al., 2000). In all, the concordant immune activation and anti-inflammatory responses induced by NKTT320 may mean that there is a potential *in vivo* for eliciting potent inflammatory responses without excessive or non-resolving immune activation. This remains to be tested in both long-term studies and in the context of vaccination or infection.

In summary, the current studies detailed here investigate the use of NKTT320, an iNKT-specific humanized monoclonal antibody, for *in vivo* iNKT activation for the first time in the NHP model. We found, through multiple modes of investigation, that this antibody directly affects iNKT without inducing anergy and subsequently transactivates other immune subsets, most strikingly monocytes and macrophages. *In vivo* NKTT320 administration induces potent functional changes in both T cell and non T cell subsets that may influence both innate and adaptive immunity. It also triggers a balanced immune response with induction of anti-inflammatory responses to balance immune activation. The long half-life of NKTT320 as well as detection of effects on iNKT functionality well beyond the duration of detectable plasma NKTT320 indicates that this therapeutic modality would be feasible in human studies or in a translational setting. NKTT320 is a promising iNKT activating agent with translational potential that should be studied further for efficacy as a vaccine adjuvant and immunotherapeutic tool.

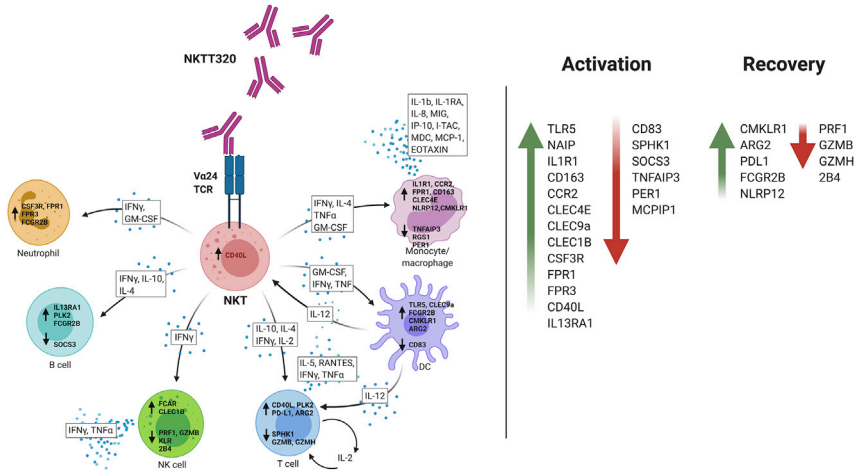

Figure 9. Schematic of NKTT320-mediated immune modulation. Schematic effect of NKTT320 on iNKT and downstream immune cell subsets as measured by Luminex, ICS, and RNA-Seq. Genes and secreted molecules are placed according to potential cellular sources. Created with BioRender.com

Limitations of the study

The present study provides the first comprehensive characterization of the *in vivo* effects of a humanized NKT-activating monoclonal antibody and raises the possibility of its utility as an immunotherapeutic agent and vaccine adjuvant. The main limitation of the current study is the lack of direct comparison of the *in vivo* effects of NKTT320 and the prototypical sphingolipid agonist αGC in our non-human primate model. The absence of vaccine experiments to demonstrate NKTT320's effect on potentiation of antigen-specific humoral and cellular immunity is another limitation to conclusions regarding potential adjuvant role of NKTT320. Future studies on NKTT320 in the context of vaccination are needed to assess its potential as an adjuvant. In addition, further studies are needed to understand the biologic effects of NKTT320 on direct iNKT TCR interactions with CD1d-expressing APCs and target cells, and its impact on induction of antigen-specific $CD8^{+}$T cell and antibody responses and tumor killing. Despite these limitations, the data presented in this study lays the necessary groundwork for future comparative studies to investigate the utility of NKTT320 as an immunotherapeutic tool for *in vivo* NKT manipulation.

STAR★METHODS

Detailed methods are provided in the online version of this paper and include the following:

- KEY RESOURCES TABLE
- RESOURCE AVAILABILITY
  - Lead contact
  - Materials availability
  - Data and code availability
- EXPERIMENTAL MODEL AND SUBJECT DETAILS
  - Ethics statement for *in vivo* non-human primate studies
  - Animals and study design
  - Processing of peripheral blood and tissues
- METHOD DETAILS
  - NKTT320 ELISA
  - Cells and reagents
  - iNKT detection
  - *In vitro* iNKT stimulation
  - Intracellular cytokine staining
  - Calcein-AM cytotoxicity assay
  - Degranulation assay
  - Proliferation assays

- Luminex
- RNA-seq

- QUANTIFICATION AND STATISTICAL ANALYSIS

SUPPLEMENTAL INFORMATION

Supplemental information can be found online at https://doi.org/10.1016/j.isci.2022.103889.

ACKNOWLEDGMENTS

We would like to acknowledge TNPRC Veterinary Medicine Staff for caring for the animals, TNPRC Flow Cytometry Core for acquiring flow cytometry data, and the TNPRC Pathogen Detection and Quantification Core for reading and analyzing the Luminex plates. We thank Cathy Flemington, Alanna Wanek, Dr. Kejing Song, and Dr. Jay Kolls in the Tulane Center for Translational Research in Infection & Inflammation NextGen Sequencing Core for assistance with the RNA-Seq studies. We thank Dr. Leonid Metelitsa for the A4.4 cell line. We would like to acknowledge Dr. Mark Exley for thoughtful discussion. The study was funded by NIH/NIAID R01 AI102693 (AK), R21 AI145642 (AK) and P51 OD011104. The authors would like to thank the NIH Tetramer Core facility for provision of the CD1dTM conjugated to both APC and BV421.

AUTHOR CONTRIBUTIONS

Conceptualization: AK, NB; Investigation: NB, SY, NR, DT, ES, TFS, LS; Formal Analysis: NB, MF, JM, RS, AK; Resources: RS; Writing-Original Draft: NB, AK; Writing-Review & Editing: NB, AK, MF, NR, SY, RS, JM; Supervision: AK; Funding Acquisition: AK.

DECLARATION OF INTERESTS

Dr. Robert Schaub's former employment with NKT Therapeutics, the manufacturer of NKTT320, may be considered a potential conflict of interest.

Received: June 30, 2021
Revised: December 22, 2021
Accepted: February 4, 2022
Published: March 18, 2022

REFERENCES

Andrews, S. (2010). FastQC: a quality control tool for high throughput sequence data. http://www.bioinformatics.babraham.ac.uk/projects/fastqc/.

Adada, M.M., Orr-Gandy, K.A., Snider, A.J., Canals, D., Hannun, Y.A., Obeid, L.M., and Clarke, C.J. (2013). Sphingosine kinase 1 regulates tumor necrosis factor-mediated RANTES induction through p38 mitogen-activated protein kinase but independently of nuclear factor kappaB activation. J. Biol. Chem. *288*, 27667–27679.

Anders, S., and Huber, W. (2010). Differential expression analysis for sequence count data. Genome Biol. *11*, R106.

Ashburner, M., Ball, C.A., Blake, J.A., Botstein, D., Butler, H., Cherry, J.M., Davis, A.P., Dolinski, K., Dwight, S.S., Eppig, J.T., et al. (2000). Gene Ontology: tool for the unification of biology. Nat. Genet. *25*, 25–29.

Asosingh, K., Lauruschkat, C.D., Alemagno, M., Frimel, M., Wanner, N., Weiss, K., Kessler, S., Meyers, D.A., Bennett, C., Xu, W., and Erzurum, S. (2020). Arginine metabolic control of airway inflammation. JCI Insight *5*, e127801.

Bainbridge, T.W., Dealmeida, V.I., Izrael-Tomasevic, A., Chalouni, C., Pan, B., Goldsmith, J., Schoen, A.P., Quinones, G.A., Kelly, R., Lill, J.R., et al. (2014). Evolutionary divergence in the catalytic activity of the CAM-1, ROR1 and ROR2 kinase domains. PLoS ONE *9*, e102695.

Bates, J.M., Flanagan, K., Mo, L., Ota, N., Ding, J., Ho, S., Liu, S., Roose-Girma, M., Warming, S., and Diehl, L. (2015). Dendritic cell CD83 homotypic interactions regulate inflammation and promote mucosal homeostasis. Mucosal Immunol. *8*, 414–428.

Bendelac, A., Savage, P.B., and Teyton, L. (2007). The biology of NKT cells. Annu. Rev. Immunol. *25*, 297–336.

Berzins, S.P., Smyth, M.J., and Baxter, A.G. (2011). Presumed guilty: natural killer T cell defects and human disease. Nat. Rev. Immunol. *11*, 131–142.

Bolger, A.M., Lohse, M., and Usadel, B. (2014). Trimmomatic: a flexible trimmer for illumina sequence data. Bioinformatics *30*, 2114–2120.

Brennan, P.J., Brigl, M., and Brenner, M.B. (2013). Invariant natural killer T cells: an innate activation scheme linked to diverse effector functions. Nat. Rev. Immunol. *13*, 101–117.

Bricard, G., Venkataswamy, M.M., Yu, K.O., Im, J.S., Ndonye, R.M., Howell, A.R., Veerapen, N., Illarionov, P.A., Besra, G.S., Li, Q., et al. (2010). A-galactosylceramide analogs with weak agonist activity for human iNKT cells define new candidate anti-inflammatory agents. PLoS ONE *5*, e14374.

Bromley, S.K., Mempel, T.R., and Luster, A.D. (2008). Orchestrating the orchestrators: chemokines in control of T cell traffic. Nat. Immunol. *9*, 970–980.

Caminschi, I., Proietto, A.I., Ahmet, F., Kitsoulis, S., Shin Teh, J., Lo, J.C., Rizzitelli, A., Wu, L., Vremec, D., Van Dommelen, S.L., et al. (2008). The dendritic cell subtype-restricted C-type lectin Clec9A is a target for vaccine enhancement. Blood *112*, 3264–3273.

Carnaud, C., Lee, D., Donnars, O., Park, S.H., Beavis, A., Koezuka, Y., and Bendelac, A. (1999). Cutting edge: cross-talk between cells of the innate immune system: NKT cells rapidly activate NK cells. J. Immunol. *163*, 4647–4650.

Chang, D.H., Osman, K., Connolly, J., Kukreja, A., Krasovsky, J., Pack, M., Hutchinson, A., Geller, M., Liu, N., Annable, R., et al. (2005). Sustained expansion of NKT cells and antigen-specific T cells after injection of alpha-galactosyl-ceramide loaded mature dendritic cells in cancer patients. J. Exp. Med. *201*, 1503–1517.

Chang, P.P., Barral, P., Fitch, J., Pratama, A., Ma, C.S., Kallies, A., Hogan, J.J., Cerundolo, V., Tangye, S.G., Bittman, R., et al. (2011). Identification of Bcl-6-dependent follicular helper NKT cells that provide cognate help for B cell responses. Nat. Immunol. *13*, 35–43.

Chen, N., Mccarthy, C., Drakesmith, H., Li, D., Cerundolo, V., Mcmichael, A.J., Screaton, G.R., and Xu, X.N. (2006). HIV-1 down-regulates the expression of CD1d via Nef. Eur. J. Immunol. *36*, 278–286.

Cueto, F.J., del Fresno, C., and Sancho, D. (2019). DNGR-1, a dendritic cell-specific sensor of tissue damage that dually modulates immunity and inflammation. Front. Immunol. *10*, 3146.

Dahlgren, C., Holdfeldt, A., Lind, S., Martensson, J., Gabl, M., Bjorkman, L., Sundqvist, M., and Forsman, H. (2020). Neutrophil signaling that challenges dogmata of G protein-coupled receptor regulated functions. ACS Pharmacol. Transl. Sci. *3*, 203–220.

Damouche, A., Lazure, T., Avettand-Fènoël, V., Huot, N., Dejucq-Rainsford, N., Satie, A.P., Mélard, A., David, L., Gommet, C., Ghosn, J., et al. (2015). Adipose tissue is a neglected viral reservoir and an inflammatory site during chronic HIV and SIV infection. PLoS Pathog. *11*, e1005153.

Das, T., Chen, Z., Hendriks, R.W., and Kool, M. (2018). A20/Tumor necrosis factor alpha-induced protein 3 in immune cells controls development of autoinflammation and autoimmunity: lessons from mouse models. Front. Immunol. *9*, 104.

Deshmane, S.L., Kremlev, S., Amini, S., and Sawaya, B.E. (2009). Monocyte chemoattractant protein-1 (MCP-1): an overview. J. Interferon Cytokine Res. *29*, 313–326.

Dobin, A., Davis, C.A., Schlesinger, F., Drenkow, J., Zaleski, C., Jha, S., Batut, P., Chaisson, M., and Gingeras, T.R. (2013). STAR: ultrafast universal RNA-seq aligner. Bioinformatics *29*, 15–21.

Dowling, J.K., Afzal, R., Gearing, L.J., Cervantes-Silva, M.P., Annett, S., Davis, G.M., de Santi, C., Assmann, N., Dettmer, K., Gough, D.J., et al. (2021). Mitochondrial arginase-2 is essential for IL-10 metabolic reprogramming of inflammatory macrophages. Nat. Commun. *12*, 1460.

Eissmann, P., Beauchamp, L., Wooters, J., Tilton, J.C., Long, E.O., and Watzl, C. (2005). Molecular basis for positive and negative signaling by the natural killer cell receptor 2B4 (CD244). Blood *105*, 4722–4729.

Exley, M., Garcia, J., Balk, S.P., and Porcelli, S. (1997). Requirements for CD1d recognition by human invariant Valpha24+ CD4-CD8- T cells. J. Exp. Med. *186*, 109–120.

Exley, M.A., Hou, R., Shaulov, A., Tonti, E., Dellabona, P., Casorati, G., Akbari, O., Akman, H.O., Greenfield, E.A., Gumperz, J.E., et al. (2008). Selective activation, expansion, and monitoring of human iNKT cells with a monoclonal antibody specific for the TCR alpha-chain CDR3 loop. Eur. J. Immunol. *38*, 1756–1766.

Fernandez, C.S., Jegaskanda, S., Godfrey, D.I., and Kent, S.J. (2013). In-vivo stimulation of macaque natural killer T cells with alpha-galactosylceramide. Clin. Exp. Immunol. *173*, 480–492.

Field, J.J., Majerus, E., Ataga, K.I., Vichinsky, E.P., Schaub, R., Mashal, R., and Nathan, D.G. (2017). NNKTT120, an anti-iNKT cell monoclonal antibody, produces rapid and sustained iNKT cell depletion in adults with sickle cell disease. PLoS ONE *12*, e0171067.

Finlay, D., and Cantrell, D. (2011). The coordination of T-cell function by serine/threonine kinases. Cold Spring Harb. Perspect. Biol. *3*, a002261.

Freeman, G.J., Long, A.J., Iwai, Y., Bourque, K., Chernova, T., Nishimura, H., Fitz, L.J., Malenkovich, N., Okazaki, T., Byrne, M.C., et al. (2000). Engagement of the PD-1 immunoinhibitory receptor by a novel B7 family member leads to negative regulation of lymphocyte activation. J. Exp. Med. *192*, 1027–1034.

Fujii, S., Liu, K., Smith, C., Bonito, A.J., and Steinman, R.M. (2004). The linkage of innate to adaptive immunity via maturing dendritic cells in vivo requires CD40 ligation in addition to antigen presentation and CD80/86 costimulation. J. Exp. Med. *199*, 1607–1618.

Fujii, S., Shimizu, K., Kronenberg, M., and Steinman, R.M. (2002). Prolonged IFN-gamma-producing NKT response induced with alpha-galactosylceramide-loaded DCs. Nat. Immunol. *3*, 867–874.

Fujii, S., Shimizu, K., Smith, C., Bonifaz, L., and Steinman, R.M. (2003). Activation of natural killer T cells by alpha-galactosylceramide rapidly induces the full maturation of dendritic cells in vivo and thereby acts as an adjuvant for combined CD4 and CD8 T cell immunity to a coadministered protein. J. Exp. Med. *198*, 267–279.

Fullerton, J.N., and Gilroy, D.W. (2016). Resolution of inflammation: a new therapeutic frontier. Nat. Rev. Drug Discov. *15*, 551–567.

Furukawa, A., Kamishikiryo, J., Mori, D., Toyonaga, K., Okabe, Y., Toji, A., Kanda, R., Miyake, Y., Ose, T., Yamasaki, S., and Maenaka, K. (2013). Structural analysis for glycolipid recognition by the C-type lectins Mincle and MCL. Proc. Natl. Acad. Sci. U S A *110*, 17438–17443.

Gaya, M., Barral, P., Burbage, M., Aggarwal, S., Montaner, B., Warren Navia, A., Aid, M., Tsui, C., Maldonado, P., Nair, U., et al. (2018). Initiation of antiviral B cell immunity relies on innate signals from spatially positioned NKT cells. Cell *172*, 517–533.e20.

Geiger, R., Rieckmann, J.C., Wolf, T., Basso, C., Feng, Y., Fuhrer, T., Kogadeeva, M., Picotti, P., Meissner, F., Mann, M., et al. (2016). L-arginine modulates T cell metabolism and enhances survival and anti-tumor activity. Cell *167*, 829–842.e13.

Giaccone, G., Punt, C.J., Ando, Y., Ruijter, R., Nishi, N., Peters, M., Von Blomberg, B.M., Scheper, R.J., Van der Vliet, H.J., Van den Eertwegh, A.J., et al. (2002). A phase I study of the natural killer T-cell ligand alpha-galactosylceramide (KRN7000) in patients with solid tumors. Clin. Cancer Res. *8*, 3702–3709.

Gonzalez-Aseguinolaza, G., van Kaer, L., Bergmann, C.C., Wilson, J.M., Schmieg, J., Kronenberg, M., Nakayama, T., Taniguchi, M., Koezuka, Y., and Tsuji, M. (2002). Natural killer T cell ligand alpha-galactosylceramide enhances protective immunity induced by malaria vaccines. J. Exp. Med. *195*, 617–624.

Gout, E., Garlatti, V., Smith, D.F., Lacroix, M., Dumestre-Perard, C., Lunardi, T., Martin, L., Cesbron, J.Y., Arlaud, G.J., Gaboriaud, C., and Thielens, N.M. (2010). Carbohydrate recognition properties of human ficolins: glycan array screening reveals the sialic acid binding specificity of M-ficolin. J. Biol. Chem. *285*, 6612–6622.

Heinrich, P.C., Behrmann, I., Muller-Newen, G., Schaper, F., and Graeve, L. (1998). Interleukin-6-type cytokine signalling through the gp130/Jak/STAT pathway. Biochem. J. *334*, 297–314.

Huysamen, C., and Brown, G.D. (2009). The fungal pattern recognition receptor, Dectin-1, and the associated cluster of C-type lectin-like receptors. FEMS Microbiol. Lett. *290*, 121–128.

Hwangbo, C., Tae, N., Lee, S., Kim, O., Park, O.K., Kim, J., Kwon, S.H., and Lee, J.H. (2016). Syntenin regulates TGF-beta1-induced smad activation and the epithelial-to-mesenchymal transition by inhibiting caveolin-mediated TGF-beta type I receptor internalization. Oncogene *35*, 389–401.

Jura, J., Skalniak, L., and Koj, A. (2012). Monocyte chemotactic protein-1-induced protein-1 (MCPIP1) is a novel multifunctional modulator of inflammatory reactions. Biochim. Biophys. Acta *1823*, 1905–1913.

Kato, Y., Zaid, A., Davey, G.M., Mueller, S.N., Nutt, S.L., Zotos, D., Tarlinton, D.M., Shortman, K., Lahoud, M.H., Heath, W.R., and Caminschi, I. (2015). Targeting antigen to Clec9A primes follicular Th cell memory responses capable of robust recall. J. Immunol. *195*, 1006–1014.

Kim, D., Pertea, G., Trapnell, C., Pimentel, H., Kelley, R., and Salzberg, S.L. (2013). TopHat2: accurate alignment of transcriptomes in the presence of insertions, deletions and gene fusions. Genome Biol. *14*, R36.

King, I.L., Fortier, A., Tighe, M., Dibble, J., Watts, G.F., Veerapen, N., Haberman, A.M., Besra, G.S., Mohrs, M., Brenner, M.B., and Leadbetter, E.A. (2011). Invariant natural killer T cells direct B cell responses to cognate lipid antigen in an IL-21-dependent manner. Nat. Immunol. *13*, 44–50.

Kolde, R. (2019). Pheatmap: pretty heatmaps. https://CRAN.R-project.org/package=pheatmap.

Kopecky-Bromberg, S.A., Fraser, K.A., PICA, N., Carnero, E., Moran, T.M., Franck, R.W., Tsuji, M., and Palese, P. (2009). Alpha-C-galactosylceramide as an adjuvant for a live attenuated influenza virus vaccine. Vaccine *27*, 3766–3774.

Kunii, N., Horiguchi, S., Motohashi, S., Yamamoto, H., Ueno, N., Yamamoto, S., Sakurai, D., Taniguchi, M., Nakayama, T., and Okamoto, Y. (2009). Combination therapy of in vitro-expanded natural killer T cells and alpha-galactosylceramide-pulsed antigen-presenting cells in patients with recurrent head and neck carcinoma. Cancer Sci. *100*, 1092–1098.

Lee, Y.J., Wang, H., Starrett, G.J., Phuong, V., Jameson, S.C., and Hogquist, K.A. (2015). Tissue-specific distribution of iNKT cells impacts their cytokine response. Immunity *43*, 566–578.

Liberzon, A., Subramanian, A., Pinchback, R., Thorvaldsdóttir, H., Tamayo, P., and Mesirov, J.P. (2011). Molecular signatures database (MSigDB) 3.0. Bioinformatics *27*, 1739–40.

Liu, Y., Beyer, A., and Aebersold, R. (2016). On the dependency of cellular protein levels on mRNA abundance. Cell *165*, 535–550.

Lynch, L. (2014). Adipose invariant natural killer T cells. Immunology *142*, 337–346.

Martens, M., Ammar, A., Riutta, A., Waagmeester, A., Slenter, Denise N., Hanspers, K., A. Miller, R., Digles, D., Lopes, Elisson N., Ehrhart, F., et al. (2020). WikiPathways: connecting communities. *Nucleic Acids Res. 49*, D613–D621.

McCormick, S.M., and Heller, N.M. (2015). Commentary: IL-4 and IL-13 receptors and signaling. Cytokine *75*, 38–50.

McGovern, N., Shin, A., Low, G., Low, D., Duan, K., Yao, L.J., Msallam, R., Low, I., Shadan, N.B., Sumatoh, H.R., et al. (2017). Human fetal dendritic cells promote prenatal T-cell immune suppression through arginase-2. Nature *546*, 662–666.

Moestrup, S.K., and Moller, H.J. (2004). CD163: a regulated hemoglobin scavenger receptor with a role in the anti-inflammatory response. Ann. Med. *36*, 347–354.

Moll, M., Andersson, S.K., Smed-Sorensen, A., and Sandberg, J.K. (2010). Inhibition of lipid antigen presentation in dendritic cells by HIV-1 Vpu interference with CD1d recycling from endosomal compartments. Blood *116*, 1876–1884.

Monteiro, R.C., and Van de Winkel, J.G. (2003). IgA Fc receptors. Annu. Rev. Immunol. *21*, 177–204.

Motohashi, S., Okamoto, Y., Yoshino, I., and Nakayama, T. (2011). Anti-tumor immune responses induced by iNKT cell-based immunotherapy for lung cancer and head and neck cancer. Clin. Immunol. *140*, 167–176.

Motsinger, A., Haas, D.W., Stanic, A.K., Van Kaer, L., Joyce, S., and Unutmaz, D. (2002). CD1d-restricted human natural killer T cells are highly susceptible to human immunodeficiency virus 1 infection. J. Exp. Med. *195*, 869–879.

Newman, R., Hariharan, K., Reff, M., Anderson, D.R., Braslawsky, G., Santoro, D., Hanna, N., Bugelski, P.J., Brigham-Burke, M., Crysler, C., et al. (2001). Modification of the Fc region of a primatized IgG antibody to human CD4 retains its ability to modulate CD4 receptors but does not deplete CD4(+) T cells in chimpanzees. Clin. Immunol. *98*, 164–174.

Nimmerjahn, F., and Ravetch, J.V. (2008). Fcgamma receptors as regulators of immune responses. Nat. Rev. Immunol. *8*, 34–47.

Normand, S., Waldschmitt, N., Neerincx, A., Martinez-Torres, R.J., Chauvin, C., Couturier-Maillard, A., Boulard, O., Cobret, L., Awad, F., Huot, L., et al. (2018). Proteasomal degradation of NOD2 by NLRP12 in monocytes promotes bacterial tolerance and colonization by enteropathogens. Nat. Commun. *9*, 5338.

O'Leary, N.A., Wright, M.W., Brister, J.R., Ciufo, S., Haddad, D., Mcveigh, R., Rajput, B., Robbertse, B., Smith-White, B., Ako-Adjei, D., et al. (2016). Reference sequence (RefSeq) database at NCBI: current status, taxonomic expansion, and functional annotation. Nucleic Acids Res. *44*, D733–D745.

Ohira, T., Arita, M., Omori, K., Recchiuti, A., Van Dyke, T.E., and Serhan, C.N. (2010). Resolvin E1 receptor activation signals phosphorylation and phagocytosis. J. Biol. Chem. *285*, 3451–3461.

Parekh, V.V., Wilson, M.T., Olivares-Villagómez, D., Singh, A.K., Wu, L., Wang, C.R., Joyce, S., and Van Kaer, L. (2005). Glycolipid antigen induces long-term natural killer T cell anergy in mice. J. Clin. Invest. *115*, 2572–2583.

Patel, N.P., Guan, P., Bahal, D., Hashem, T., Scheuplein, F., Schaub, R., Nichols, K.E., and Das, R. (2020). Cancer immunotherapeutic potential of NKTT320, a novel, invariant, natural killer T cell-activating, humanized monoclonal antibody. Int. J. Mol. Sci. *21*, 4317.

Reddy, M.P., Kinney, C.A., Chaikin, M.A., Payne, A., Fishman-Lobell, J., Tsui, P., Dal Monte, P.R., Doyle, M.L., Brigham-Burke, M.R., Anderson, D., et al. (2000). Elimination of Fc receptor-dependent effector functions of a modified IgG4 monoclonal antibody to human CD4. J. Immunol. *164*, 1925–1933.

Robinson, M.D., Mccarthy, D.J., and Smyth, G.K. (2010). edgeR: a bioconductor package for differential expression analysis of digital gene expression data. Bioinformatics *26*, 139–140.

Roederer, M., Nozzi, J.L., and Nason, M.C. (2011). SPICE: exploration and analysis of post-cytometric complex multivariate datasets. Cytometry *79*, 167–174.

Rout, N., Else, J.G., Yue, S., Connole, M., Exley, M.A., and Kaur, A. (2010). Paucity of CD4+ natural killer T (NKT) lymphocytes in sooty mangabeys is associated with lack of NKT cell depletion after SIV infection. PLoS ONE *5*, e9787.

Rout, N., Greene, J., Yue, S., O'connor, D., Johnson, R.P., Else, J.G., Exley, M.A., and Kaur, A. (2012). Loss of effector and anti-inflammatory natural killer T lymphocyte function in pathogenic simian immunodeficiency virus infection. PLoS Pathog. *8*, e1002928.

Saltiel, A.R., and Olefsky, J.M. (2017). Inflammatory mechanisms linking obesity and metabolic disease. J. Clin. Invest. *127*, 1–4.

Scheuplein, F., Thariath, A., Macdonald, S., Truneh, A., Mashal, R., and Schaub, R. (2013). A humanized monoclonal antibody specific for invariant natural killer T (iNKT) cells for in vivo depletion. PLoS ONE *8*, e76692.

Schmieder, R., and Edwards, R. (2011). Quality control and preprocessing of metagenomic datasets. Bioinformatics *27*, 863–864.

Silk, J.D., Hermans, I.F., Gileadi, U., Chong, T.W., Shepherd, D., Salio, M., Mathew, B., Schmidt, R.R., Lunt, S.J., Williams, K.J., et al. (2004). Utilizing the adjuvant properties of CD1d-dependent NK T cells in T cell-mediated immunotherapy. J. Clin. Invest. *114*, 1800–1811.

Somanchi, S.S., Mcculley, K.J., Somanchi, A., Chan, L.L., and Lee, D.A. (2015). A novel method for assessment of natural killer cell cytotoxicity using image cytometry. PLoS ONE *10*, e0141074.

Stober, D., Jomantaite, I., Schirmbeck, R., and Reimann, J. (2003). NKT cells provide help for dendritic cell-dependent priming of MHC class I-restricted CD8+ T cells in vivo. J. Immunol. *170*, 2540–2548.

Subramanian, A., Tamayo, P., Mootha, V.K., Mukherjee, S., Ebert, B.L., Gillette, M.A., Paulovich, A., Pomeroy, S.L., Golub, T.R., Lander, E.S., and Mesirov, J.P. (2005). Gene set enrichment analysis: A knowledge-based approach for interpreting genome-wide expression profiles. Proc Natl Acad Sci U S A *102*, 15545–15550.

Sugimoto, T., Morioka, N., Zhang, F.F., Sato, K., Abe, H., Hisaoka-Nakashima, K., and Nakata, Y. (2014). Clock gene Per1 regulates the production of CCL2 and interleukin-6 through p38, JNK1 and NF-kappaB activation in spinal astrocytes. Mol. Cell Neurosci. *59*, 37–46.

Tian, G., Courtney, A.N., Jena, B., Heczey, A., Liu, D., Marinova, E., Guo, L., Xu, X., Torikai, H., Mo, Q., et al. (2016). CD62L+ NKT cells have prolonged persistence and antitumor activity in vivo. J. Clin. Invest. *126*, 2341–2355.

Truneh, A., Carr, F.J., Jones, T.D., and Gresgson, J.P. (2013). Humanized Antiodies to iNKT, USA Patent Application.

Van Kaer, L., Parekh, V.V., and Wu, L. (2015). The response of CD1d-restricted invariant NKT cells to microbial pathogens and their products. Front. Immunol. *6*, 226.

Venkataswamy, M.M., Baena, A., Goldberg, M.F., Bricard, G., Im, J.S., Chan, J., Reddington, F., Besra, G.S., Jacobs, W.R., Jr., and Porcelli, S.A. (2009). Incorporation of NKT cell-activating glycolipids enhances immunogenicity and vaccine efficacy of Mycobacterium bovis bacillus Calmette-Guerin. J. Immunol. *183*, 1644–1656.

Ward, A.C. (2007). The role of the granulocyte colony-stimulating factor receptor (G-CSF-R) in disease. Front. Biosci. *12*, 608–618.

Watarai, H., Nakagawa, R., Omori-Miyake, M., Dashtsoodol, N., and Taniguchi, M. (2008). Methods for detection, isolation and culture of mouse and human invariant NKT cells. Nat. Protoc. *3*, 70–78.

Woltman, A.M., Ter Borg, M.J., Binda, R.S., Sprengers, D., Von Blomberg, B.M., Scheper, R.J., Hayashi, K., Nishi, N., Boonstra, A., Van der Molen, R., and Janssen, H.L. (2009). Alpha-galactosylceramide in chronic hepatitis B infection: results from a randomized placebo-controlled Phase I/II trial. Antivir. Ther. *14*, 809–818.

Zhao, Y., and Shao, F. (2015). The NAIP-NLRC4 inflammasome in innate immune detection of bacterial flagellin and type III secretion apparatus. Immunol. Rev. *265*, 85–102.

STAR★METHODS

KEY RESOURCES TABLE

REAGENT or RESOURCE	SOURCE	IDENTIFIER
Antibodies		
Monkey adsorbed goat anti-human IgG	Southern Biotech	Cat#2049-01; RRID: AB_2795694
Goat anti-human IgG Biotin (monkey adsorbed)	Southern Biotech	Cat#2049-08; RRID: AB_2795697
Goat anti-mouse IgG (GAM-IgG) Fab2 fragments	Seracare KPL	Cat#5210-0303
Please see Table S5 for the full list of antibodies used in Flow Cytometry experiments.		
Chemicals, peptides, and recombinant proteins		
Bromo-2′-deoxyuridine (BrdU)	BD Biosciences, Franklin Lakes, NJ	Cat#51-2420KC
Calcein AM	Life Technologies Corp, Carlsbad, CA	Cat#C3099
IL-2	Millipore Sigma, St Louis, MO	Cat#12644-5X10UG
BD GolgiPlug Protein Transport Inhibitor (Containing Monensin)	BD Biosciences, Franklin Lakes, NJ	Cat#554724; RRID: AB_2869012
BD GolgiPlug Protein Transport Inhibitor (Containing Brefeldin A)	BD Biosciences, Franklin Lakes, NJ	Cat#555029; RRID: AB_2869014
LIVE/DEAD™ Fixable Violet Dead Cell Stain Kit, for 405 nm excitation	Invitrogen, Carlsbad, CA	Cat#L34963
Fixation and Permeabilization Solution (BD Fix/Perm)	BD Biosciences, Franklin Lakes, NJ	Cat#554722; RRID: AB_2869010
Stabilizing Fixative	BD Biosciences, Franklin Lakes, NJ	Cat#338036
BD Perm/Wash Buffer	BD Biosciences, Franklin Lakes, NJ	Cat#554723; RRID: AB_2869011
Critical commercial assays		
Qiagen RNeasy Plus Mini Kit	Qiagen	Cat#74134
Zymo Clean & Concentrate-5 Kit	Zymo	Cat#R1013
Qubit RNA BR Assay Kit	Invitrogen, Carlsbad, CA	Cat#Q10210
Monkey Cytokine Magnetic 29-Plex Luminex	Invitrogen, Carlsbad, CA	Cat#LPC0005M
Deposited data		
Gene Ontology (GO) database	Gene Ontology Consortium, The Gene Ontology resource: enriching a GOld mine	Ashburner et al. (2000)
Hallmark (H) gene set of the Molecular Signature database (MsigDB)	UC San Diego and the Broad Institute	Subramanian et al. (2005) and Liberzon et al. (2011)
Curated (C2) gene set of the Molecular Signature database (MsigDB)	UC San Diego and the Broad Institute	Subramanian et al. (2005) and Liberzon et al. (2011)
WikiPathways	Wikipathways.org	Martens et al. (2020)
Deposited RNAseq raw data from our study	Tulane RNA-Seq Core	GEO: GSE194235
GRCh37/hg19 reference genome	Genome Reference Consortium	GCA_000001405.1
Experimental Models: Cell Lines		
K-562	ATCC	ATCC#CCL-243; RRID: CVCL_0004
A4.4	MTA with Dr. Leonid Metilitsa	Tian et al. (2016)
Mock transfected C1R cells (C1Rmock)	Mark Exley	Exley et al. (1997)
C1R cells stably transfected with CD1d (C1Rd)	Mark Exley	Exley et al., 1997

(*Continued on next page*)

Continued

REAGENT or RESOURCE	SOURCE	IDENTIFIER
Experimental models: organisms/strains		
Mauritian Origin Cynomolgus Macaques	Tulane National Primate Research Center Breeding Colony	N/A
Software and algorithms		
Bio-Plex Manager Software v6.2	Bio-Rad, Hercules, CA	Cat#171STND05
RNA-seq for Eukaryotes Analysis v3	Banana Slug Genomics Center at the University of California Santa Cruz	https://sluggenomicscenter.ucsc.edu/
Trimmomatic	Bolger et al. (2014)	
PRINSEQ	Schmieder and Edwards (2011)	
STAR	Kim et al. (2013) and Dobin et al. (2013)	
NCBI RefSeq	O'Leary et al. (2016)	
DESeq	Anders and Huber (2010)	
Gen5 1.11.5 Software	Agilent, Santa Clara, CA	https://www.biotek.com/products/software-robotics-software/gen5-microplate-reader-and-imager-software/
edgeR	Robinson et al. (2010)	
'pheatmap' package in R	Kolde (2019)	
GSEA was performed with the R package 'ClusterProfiler'	R	
R software package 'ggplot2'	R	
FlowJo version 9.9	Ashland, OR	https://www.flowjo.com/solutions/flowjo/downloads/v9
simplified presentation of incredibly complex evaluations (SPICE)	Roederer et al. (2011)	
BD FACSDiva version 9.1	BD Biosciences, Franklin Lakes, NJ	https://www.bdbiosciences.com/en-us/products/software/instrument-software/bd-facsdiva-software#Overview
GraphPad/PRISM	LaJolla, CA	https://www.graphpad.com/

RESOURCE AVAILABILITY

Lead contact

Further information and requests for resources and reagents should be directed to and will be fulfilled by the lead contact, Dr. Amitinder Kaur (akaur@tulane.edu).

Materials availability

This study did not generate new unique reagents.

Data and code availability

All RNA-seq data was deposited in GEO (GEO: GSE194235). No new code was generated to analyze this data set. Any additional information required to reanalyze the data reported in this paper is available from the lead contact upon request.

EXPERIMENTAL MODEL AND SUBJECT DETAILS

Ethics statement for *in vivo* non-human primate studies

In vivo non-human primate studies were performed at the New England Primate Research Center (NEPRC) (Boston, MA; 2013-2015) and the Tulane National Primate Research Center (TNPRC) (Covington, LA; 2015-2018). This study was carried out in accordance with the Guide for the Care and Use of Laboratory Animals of the NIH. The protocol was reviewed and approved by the Institutional Animal Care and Use Committees

(IACUCs) at NEPRC and TNPRC. The facilities also maintained an Animal Welfare Assurance statement with the National Institutes of Health, Office of Laboratory Animal Welfare.

Animals and study design

We longitudinally evaluated blood from adult male MCM (n = 12) and tissues from a subset of these animals (n = 3), pre and post NKTT320 treatment.

Single-dose pharmacokinetic studies. NKTT320 was administered by intravenous route at escalating doses in three groups: low (100 μg/kg, n = 6), mid (300 μg/kg, n = 3) and high (1000 μg/kg, n = 3). Samples were taken prior to NKTT320 administration, and 30 minutes, 2 hours, days 1, 3, 7, and weeks 2, 4, 6, 8, and 14 post treatment. Animals were released to the second phase of the study after the final time point.

Repeated dose studies. One animal received 3 doses of NKTT320—30 μg/kg, 100 μg/kg and 100 μg/kg—at 2-week intervals.

Toxicology. Serum AST and ALT levels were measured on the Beckman Coulter Olympus AU 480 system by the clinical pathology core at TNPRC.

Processing of peripheral blood and tissues

Peripheral blood mononuclear cells (PBMCs) were isolated from MCM by density gradient centrifugation. In brief, peripheral blood was diluted 1:1 in PBS and layered over 90% ficoll at a 1:2 ratio. The gradient was then spun at 2,200 rpm for 45 minutes with the brake off. Cells were then isolated, washed and counted according to standard methods. PBMCs were used for phenotyping and functional assays. In a subset of experiments bone marrow (BM), bronchoalveolar lavage (BAL), peripheral lymph node (PLN), rectal mucosa, subcutaneous abdominal adipose tissue biopsies were taken. In brief, tissue lymphocytes were isolated as follows. BM was treated identically to peripheral blood, described above. BAL was strained, spun at 1,500 rpm for 5 minutes and counted. PLN lymphocytes were isolated using mechanical separation. Rectal mucosa lymphocytes were isolated by enzymatic digestion with EDTA followed by collagenase II. Remaining tissue was mechanically disrupted, strained and washed before counting. Similarly, adipose tissue was initially digested using collagenase II followed by mechanical disruption, straining out remaining tissue and washing the cells before counting. Tissue lymphocytes were used to assess iNKT frequency within tissues following activation with NKTT230.

METHOD DETAILS

NKTT320 ELISA

NKT Therapeutics developed an enzyme-linked immunosorbent assay (ELISA) to determine NKTT320 concentration in monkey plasma or serum based on the detection of human IgG4. Briefly, 96 well plates were coated with monkey adsorbed goat anti-human IgG (1 μg/mL) and incubated at 37°C for 2 hours or 4°C overnight. Plates were washed 3× with wash buffer (0.05% Tween 20 in 1× PBS). Wells were blocked using 3% BSA in 1× PBS for 2 h at room temperature. Plates were washed as described above, diluted plasma samples, NKTT320 standards and controls were added and incubated for either 2 hours at room temperature or overnight at 4°C. For antibody detection, 0.1 μg/mL goat anti-human IgG Biotin (monkey adsorbed) was added to each well and incubated for 1 hour at room temperature. Plates were washed as described above, 100 μL diluted streptavidin-HRP polymer (SPP) conjugate was added, and samples were incubated 1 hour at room temperature. Plates were washed as described above, 100 μL of Tetramethylbenzidine (TMB) was added to each well, incubated in the dark for between 10-20 minutes and the reaction was stopped by adding 100 μL stop solution to each well. Plates were read at 450nm within 30 minutes of adding stop solution on a Biotek synergy 2 (Winooski, VT) microplate reader and data was acquired and analyzed using Gen5 1.11.5 software, Excel and GraphPad/PRISM.

Cells and reagents

CD1d transfectant C1R cells. C1R cells either mock transfected or stably transfected with CD1d (C1Rd) (Rout et al., 2010; Exley et al., 1997) were used either loaded with αGC (Avanti Polar Lipids; Alabaster, AL) or PBS to stimulate PBMC to compare a known iNKT specific stimulant with NKTT320 stimulation. C1R transfectants were used at a ratio of 1:10 C1R: PBMC for stimulation.

CD1d transfectant K652 cells. K652 cells stably transfected with CD1d (A4.4) cells (Tian et al., 2016) were obtained through an MTA with Dr. Leonid Metilitsa. A4.4 cells loaded with aGC were used with or without NKTT320 in a Calcein-AM release killing assay with K652 as a comparison. Target cells were used at effector: target ratios of between 2:1 and 8:1.

Alpha-galactosylceramide. αGC stock was received at 2 mg/mL from Avanti Polar Lipids, Alabaster, AL and stored in 10 μL aliquots in brown glass vials at −80°C. Aliquots of working solution of 20 μg/mL in R10 medium (RPMI + HEPES + L-glutamine+10% fetal calf serum) were stored at −20°C until use. αGC was loaded onto C1Rd cells and used for iNKT stimulation at a final concentration of 100 ng/mL.

NKTT320 monoclonal antibody. NKTT320 is a humanized monoclonal antibody developed by NKT Therapeutics (Sharon, MA) that binds to the CDR3 region of the Vα chain of the human iNKT TCR (Scheuplein et al., 2013; Patel et al., 2020, Truneh et al., 2013). NKTT320 is the sister antibody to NKTT120 (Field et al., 2017; Scheuplein et al., 2013). Briefly CD1d knock out mice, which lack iNKT-cells, were immunized with cyclic peptides from the CDR3 loop of the TCRα and screened for antibodies. One mouse monoclonal antibody designated 6B11, was identified as specific for human and non-human primate but not rodent iNKT-cells. 6B11 has demonstrated the ability to identify, purify, activate and expand iNKT-cells (Exley et al., 2008). To permit clinical evaluation, the murine mAb 6B11, was humanized and de-immunized using the "Composite Human Antibody™ Technology" (Antitope Ltd., Cambridge, UK) to a stabilized IgG4 activating antibody NKTT320. NKTT320 was evaluated by Surface Plasmon Resonance (SPR) assays to determine the binding affinity to soluble human iTCR. NKTT320 binds specifically and selectively to the human iTCR with a K_D of approximately 44 nM. Measurement of binding affinity and functional characterization of NKTT320 was performed using recombinant human invariant TCR and cells. NKTT320 was produced by Antitope LTD (Cambridge, UK) in a transfected CHO-M cell line provided by Selexis sa (Chemin des Aulx Switzerland).

Monoclonal antibodies for flow cytometry. Monoclonal antibodies were used for phenotyping and flow cytometric functional assays. Antibody clone, vendor and panel information can be found in Table S5.

iNKT detection

CD1dTMs loaded with αGC conjugated to either APC or BV421 were obtained from the NIH Tetramer core. These loaded tetramers were titrated and used at the optimal titrated volume. iNKTs are identified based on co-expression of CD1d-TM and Vα24 as described previously (Rout et al., 2010). Briefly, isolated cells were washed, incubated with titrated volumes of CD1dTM at room temperature for 30 minutes followed by addition of the remaining antibodies in the staining cocktail for 20 minutes. Standard flow cytometric protocols were used for the remaining surface or intracellular cytokine staining panels. A minimum of 2 million PBMCs were used for flow cytometric staining to allow for at least 200,000 lymphocyte events to be captured to visualize rare iNKT populations. All flow cytometry panels were run on either BD LSR-II or BD Fortessa instruments (BD, Franklin Lakes, NJ) by the TNPRC Flow Cytometry Core.

In vitro iNKT stimulation

In vitro stimulation with soluble NKTT320. Peripheral blood mononuclear cells (PBMC) isolated from 3 MCM were incubated with escalating concentrations (0.1, 1, 10 and 25ug/mL) of NKTT320 diluted in R10 media (RPMI/1%Hepes/10%FBS). Cells were incubated overnight at 37°C and harvested for Flow Cytometry staining.

In vitro stimulation with cross-linked NKTT320. PBMC were stimulated with 200 ng/mL NKTT320 cross-linked with goat-anti-mouse (GAM) IgG Fab2 fragments. Briefly wells were first coated with GAM-IgG at 2.5 ng/mL (SeraCare, formerly KPL, Gaithersburg, MD) in 50mM TRIS buffer (pH=8.6), 1mL per well, and incubated for 1 hour at 37°C. Wells were then washed 3× with PBS and 1mL/well 200 ng/mL NKTT320 in PBS was added. Plates were then incubated another hour at 37°C, washed and 1 million PBMC in R10 media were added to each well. Cells were then incubated 48 hours, harvested for flow cytometry; supernatants were harvested for Luminex assay.

In vitro stimulation with αGC. PBMC were stimulated with 100 ng/mL αGC loaded onto C1Rd cells. C1Rd cells were irradiated at 10,000 rads (100 Gy) and mixed with PBMCs at a ratio of 1:1000. Finally,

100 ng/mL αGC was added and plates were incubated 48 hours. Cells were then harvested for flow cytometry and supernatants were harvested for Luminex assay.

Intracellular cytokine staining

Cells were stained with live/dead dye for 20 minutes at room temperature, then washed with 2% FBS/PBS. Cells were then incubated in CD1d tetramer loaded with αGC for 20 minutes with no wash. The surface stain cocktail was added to the tubes, incubated for 20 minutes, and washed with 2% FBS/PBS. Cells were incubated in BD Cytofix/Cytoperm solution (BD Biosciences, Franklin Lakes, NJ) for 20 minutes followed by a wash with BD Perm/Wash Buffer (BD Biosciences, Franklin Lakes, NJ). Intracellular antibodies were then added for a 20 minute incubation, then washed with BD Perm/Wash Buffer. Cells were fixed for 1 hour with Stabilizing Fixative (BD Biosciences, Franklin Lakes, NJ) then washed in PBS. The stained cells were acquired the next day on the LSRII using BD FACSDiva version 9.1. Compensation and analysis were performed in FlowJo v10.7.

Calcein-AM cytotoxicity assay

The ability of activated iNKT cells to kill CD1d expressing cells was determined using a Calcein release assay adapted from a previously described study (Somanchi et al., 2015).

iNKT cultures. iNKT cells from n = 4 animals were expanded in culture as follows. Half of the cells were irradiated with 3000 rads, then pulsed with 10ug αGC for 1 hour at 37°C in 5% CO_2. αGC pulsed, irradiated PBMCs were then combined with the remaining PBMCs cultured in a 24 well plate in R10 media at a concentration of 2-4x10^6cells/mL at 37°C in 5% CO_2. After 24 hours, media was replaced with R10 + 200IU/mL IL-2 (Millipore Sigma, St Louis, MO). On day 3, cell cultures were half fed with R10 + IL2 media. IL-2 media was tapered off over days 7–10 leading up to the Calcein-AM release assay.

Calcein release assay. Assay was set up on day 11 of culture. Cells were plated in aliquots of 100 μL R10 media in a 96 well U-bottom plate. The number of cells plated varied for a final effector-to-target cell ratio (E:T ratio) from 2:1 to 8:1. 50 μL R10 or 50 μL R10 + NKTT320 (50 ng/50 μL) was added to appropriate wells. Target cells (A4.4, described above) cells were pre incubated with 10 μg αGC in PBS for 1 hour at 37°C in 5% CO_2, and then washed with complete RPMI. Target A4.4 (or control K562) cells were then stained with 2 μg/mL Calcein-AM (Life Technologies Corp, Carlsbad, CA) in complete RPMI. Cells were resuspended at 1 × 10^6cells/mL in Calcein-AM-staining media (Invitrogen, Carlsbad, CA) for 30 minutes at 37°C in 5% CO_2, with intermittent mixing. Target cells were washed and resuspended at 2 × 10^6 cells/mL in R10 media with no FBS. Aliquots of 50 μL of Calcein stained target cells (1 × 10^5cells) were added to appropriate wells of a 96 well U bottom plate containing effector cells (expanded iNKT cultures). Maximum and spontaneous release controls of Calcein labeled target cells were set up in triplicates using 1% Triton X-100 (final concentration) and plain media respectively. Once all cells and media were added to 96 well U bottom plate, plate was spun at 100xg for 2 minutes, then incubated at 37°C in 5%CO_2. After 6 hours, cells were gently mixed to evenly distribute released calcein into the supernatant. The plate was then spun at 400xg for 2 minutes to pellet cells and debris. 150ul of supernatant was transferred to a flat bottom translucent 96 well plate, and fluorescence was read using a BioTek Synergy2 plate reader (Ex: 485 nm/Em: 530 nm). The percent specific lysis was calculated using the formula [(Test release –Spontaneous release)/(Maximum release –Spontaneous release)] x 100.

Degranulation assay

C1Rd and C1RMock cells (described above) were irradiated at 10,000 rads in the Mark I Model 30-1 Irradiator. Irradiated cells were then pulsed in 200 ng/mL αGC and incubated at 37°C for 1 hour. Meanwhile, FACS tubes were coated with 2.5 μg/mL goat anti-mouse (GAM) IgG (Kierkegaard and Perry Lab) suspended in TRIS buffer (bioWORLD, pH 9.0, 50mM). Tubes were incubated at 37°C for 30 minutes at a 45° angle to maximize surface area. Tubes were then washed twice with phosphate-buffered saline (PBS). 200 ng/mL NKTT320 in R10 media (RPMI plus Hepes, L-glutamine, and 10% FBS) was added to each FACS tubes at 1mL per tube. Tubes were incubated with NKTT320 at 37°C for 1 hour at a 45° angle, then decanted. Frozen PBMC containing effector cells (iNKT) were thawed and added to the coated tubes at 1x10^6 cells per tube. Irradiated, αGC pulsed C1RD and C1R Mock cells were added to their respective tubes at 1 × 10^5 cells per tube. CD107a and CD107b antibodies and 0.67 μL/mL Monensin (BD Biosciences) were added at this time. Cells were incubated at 37°C for 1 hour at a 45°angle. Finally, Brefeldin A (BD

Biosciences) was added at 0.6 μL/mL and incubated at 37°C for either 6 or 13 hours at a 45° angle. The following day, the stimulated cell suspensions were washed with PBS and stained with a degranulation flow cytometry panel (see Table S5).

Proliferation assays

In vitro proliferation assays were conducted to assess iNKT proliferative ability and anergy following multiple *in vivo* doses of NKTT320. PBMC from days 0, 1, 7, 14 following each dose of NKTT320 were assessed. One million PBMC per condition were stimulated with either R10 media, aGC or staphylococcal enterotoxin B (SEB) (Sigma, Saint Louis, MO). Cells were seeded at 0.2M per well in a 96-well plate and brought up to 200 μL/well with R10, 100 ng/mL αGC or 200 ng/mL SEB. Plates were incubated at 37°C for 5–6 days and 10uM Bromo-2′-deoxyuridine (BrdU, vendor) was added to each well 24 hours prior to staining. On the 6-7th day of incubation, cells were pooled by time-point and stimulation condition and analyzed by flow cytometry.

Luminex

Luminex technology was used to assess plasma chemokine and cytokine levels following NKTT320 treatment in 12 MCM. We used the Invitrogen (Carlsbad, CA) magnetic bead Monkey Cytokine Magnetic 29-Plex Panel covering the following analytes: EGF, HGF, VEGF, MIG, RANTES, Eotaxin, IL-8, GM-CSF, TNF alpha, IL-1 beta, IL-2, IL-4, IL-5, IL-6, IL-10, IL-12, MIP-1 alpha, IL-17, MIP-1 beta, IP-10, IL-15, MCP-1, G-CSF, IFN gamma, FGF-Basic, IL-1RA, MDC, MIF, I-TAC. Final reactions were read on a Bio-Plex® 200 System (Bio-Rad Laboratories, Hercules, CA) results were calculated using Bio-Plex Manager™ Software v6.2 (Bio-Rad) by the TNPRC Pathogen Quantification and Detection Core.

RNA-seq

Sample preparation for RNA-Seq. RNA was extracted from snap frozen, unfractionated PBMCs using the Qiagen RNeasy Plus Mini Kit (Qiagen 74,134). Briefly, cells were first thawed and pelleted, then lysed following the kit protocol. gDNA was removed using a gDNA Eliminator spin column, and remaining flow through was added to a RNeasy spin column to bind RNA. The spin column/RNA was washed, RNA was eluted and stored at −80°C. Later, samples were concentrated using Zymo Clean & Concentrate-5 Kit (R1013). Briefly, RNA was thawed, bound, and added to the Zymo-Spin IC Column. Then RNA bound to the column was washed, eluted, aliquoted and stored at −80°C. Samples were then submitted for RNA-Seq analysis using a high output, and single read 75 cycle run. Prior to Illumina total RNA library construction, DNase treated RNA was quantitated using the Qubit RNA BR assay kit (ThermoFisher Scientific, #Q10210). RNA quality (RIN) was determined on an Agilent 2100 Bioanalyzer using an Agilent RNA 6000 Nano kit (Agilent, #5067-1511). Cytoplasmic and mitochondrial rRNA was removed from each sample following the Ribo-Zero Gold rRNA Removal Kit Reference Guide from Illumina. After RNA clean up, samples were resuspended in 11ul Elution buffer followed by prime and fragmentation. Illumina compatible total RNA cDNA libraries were generated following the TruSeq Stranded Total RNA Sample Preparation Guide (Illumina #20020596). Samples were fun on an Illumina HiSeq Instrument. Raw and processed RNA-seq data was submitted to GEO (GEO: GSE194235).

RNA-seq data analysis. RNA-seq for Eukaryotes Analysis v3 was used for sequencing analysis and built by the Banana Slug Genomics Center at the University of California Santa Cruz. First, an Illumina sequencer at the Tulane School of Medicine Genomics Core was used to construct raw sequencing reads which were checked for quality and contaminants using FastQC (Andrews, 2010). Next, Trimmomatic was used to trim adapter sequences and primers from the sequencing reads (Bolger et al., 2014). Removal of polyA tail, polyN, and read segments with a quality score below 28 was accomplished by using PRINSEQ (Schmieder and Edwards, 2011). Following trimming, any reads of length less than 20bp were removed. Quality check was repeated, and high-quality reads were then mapped to the GRCh37/hg19 reference genome using STAR (Kim et al., 2013; Dobin et al., 2013) with NCBI RefSeq (O'Leary et al., 2016) annotated genes transcriptome index data. Raw read counts were normalized across all samples and then used for differential expression analysis using DE-Seq (Anders and Huber, 2010) and edgeR (Robinson et al., 2010) separately. Genes related to the immune system and with p values of <0.05 from the edgeR pipeline were identified and categorized by major cell type, which were then plotted on individual heatmaps. Heatmaps were constructed using $\log_2$ fold change data and using the 'pheatmap' package in R (Kolde, 2019).

Gene set enrichment analysis. GSEA was performed with the R package 'ClusterProfiler' at default parameters. Enrichment scores were calculated against the following 4 pathway databases containing a priori-defined gene sets: Gene Ontology (GO) database, Hallmark (H) and Curated (C2) gene sets of the Molecular Signature database (MsigDB), and WikiPathways. Gene sets significantly enriched in the datasets ($p < 0.05$) were subsequently curated for those relevant to NKT cell biological function. Enrichment plot was generated with the R software package 'ggplot2' and heatmaps with the 'pheatmap' package.

QUANTIFICATION AND STATISTICAL ANALYSIS

All flow cytometry data were analyzed using FlowJo version 9.9 (Ashland, Oregon). Cytokine polyfunctionality analyses were done using simplified presentation of incredibly complex evaluations (SPICE) (Roederer et al., 2011). Graphs were generated, and t-tests were performed using GraphPad/PRISM (LaJolla, CA). Statistical analyses were performed in GraphPad/PRISM using the non-parametric Wilcoxon Signed Rank test or paired t-test. Details of statistical analyses can be found in the figure legends. Significance was defined as $p < 0.05$. *<0.05, **<0.01, ***<0.001, ****<0.0001.